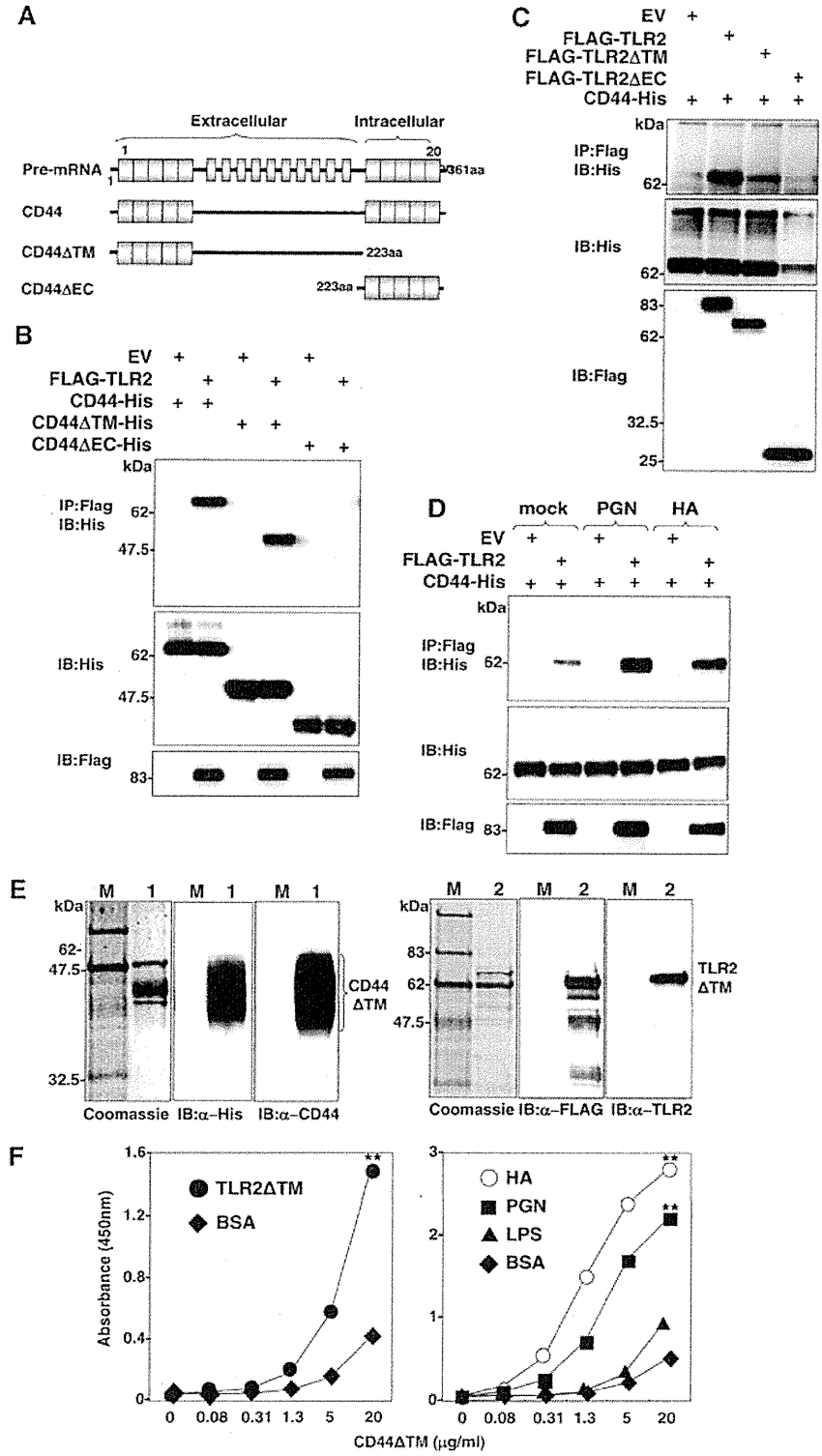

FIG 7 CD44 and TLR2 interact through their extracellular domains. (A) Structures of CD44 and its mutants used in this study. (B) FLAG-TLR2 was coexpressed with CD44-His, its mutants, or empty vector (EV) in 293T cells and immunoprecipitated with anti-FLAG antibody, and the precipitates were determined by immunoblotting (IB) with anti-His antibody. (C) CD44-His was coexpressed with FLAG-TLR2, its mutants, or empty vector in 293T cells and subjected to immunoprecipitation and immunoblotting using the appropriate antibodies. (D) Flag-TLR2 was coexpressed with CD44-His in 293T cells, stimulated with 20 μg/ml PGN or 500 μg/ml HA at 36 h posttransfection, and subjected to immunoprecipitation and immunoblotting using the appropriate antibodies at 24 h after stimulation. (E) Purified CD44ΔTM (lanes 1) and TLR2ΔTM (lanes 2) were examined by Coomassie staining and immunoblotting using antitag and specific antibodies. M denotes molecular mass markers. (F) Microtiter wells were coated with 20 μg/ml TLR2ΔTM (closed circles), 50 μg/ml HA (open circles), 40 μg/ml PGN (closed squares), 40 μg/ml LPS (closed triangles), or 50 μg/ml BSA (closed diamonds) at 4°C overnight and then incubated with the indicated concentrations of CD44ΔTM at room temperature for 1 h. The binding of CD44ΔTM was determined by measuring the absorbance at 450 nm. Asterisks indicate significant differences (*, $P < 0.05$; **, $P < 0.01$) versus the results for wells treated with BSA.

production upon stimulation with HA through an engagement with TLR2 and that the enhancement of CD44 expression was observed in the HCV replicon-harboring cells of genotypes 1b and 2a but not in cells infected with HCVcc (genotype 2a, JFH1 strain). We do not know the reason why CD44 expression was enhanced in the replicon-harboring cells but not in cells infected with HCVcc, despite the identical origin of the viral genome. Continuous replication of the HCV genome might be required for the enhancement of CD44 expression in the replicon-harboring cells autonomously replicating the HCV genome, in contrast to HCVcc-infected cells exhibiting distinct cytopathic effects. To clarify the role of CD44 in the IP-10 production in cells infected with HCV in more detail, we have to await the establishment of a robust and reliable *in vitro* replication system of various HCV genotypes, especially genotypes 1b and 1a, which are associated with progressive liver injury and persistent infection.

The cellular sources of CXCR3 ligands in CHC patients would be liver parenchymal cells, hepatic stellate cells, and sinusoidal endothelial cells within the liver and infiltrated immunocompetent cells, such as lymphocytes, macrophages, and dendritic cells. We have shown previously that production of IP-10 was enhanced in the macrophage cell lines stably expressing HCV NS5A proteins in response to various TLR ligands, in contrast to the impairment of most proinflammatory cytokines and chemokines (1; also unpublished data). Although replication of HCV in the immunocompetent cells is conflicting (8, 20, 29, 39, 43), it might be feasible to speculate that IP-10 is produced in the immunocompetent cells of CHC patients.

Upon tissue injury, high-molecular-weight HA, a ubiquitously distributed extracellular matrix component, is degraded into low-molecular-weight HA, which in turn activates an inflammatory response, although the precise receptor targeted for this response is still controversial (19). On the other hand, it has been reported that CD44 is dispensable for chemokine production by stimulation with HA in macrophages (18). Interestingly, in HCV-replicating cells, IP-10 production upon stimulation with HA but not with FSL-1 requires CD44. These results suggest that IP-10 production by stimulation with endogenous TLR2 ligands may be regulated by at least two different pathways in hepatocytes of CHC patients, through CD44-dependent and -independent pathways in response to HA and ligands derived from the intestinal microbiota, respectively. The increase of HA expression in accord with the progression of liver fibrosis in CHC patients may participate in the CD44-dependent IP-10 induction. On the other hand, HCV core and NS3 proteins have been shown to induce immune activation in immunocompetent cells through a TLR2-dependent signaling pathway, suggesting that HCV proteins also participate in immune activation as exogenous ligands (6, 7). We tried to neutralize the IP-10 induction in the HCV replicon-harboring cells by using monoclonal antibodies against CD44 and TLR2. However, these antibodies exhibited no significant inhibition of IP-10 production upon stimulation with HA (data not shown), probably due to lack of inhibition of the interaction between ligands and receptors. Furthermore, pretreatment with PGN exhibited no effect on the binding of HA to CD44 (data not shown), suggesting that the TLR2 agonist and HA bind to different regions of CD44. Further studies are needed to clarify the relationship between TLR2 and CD44 for IP-10 production in the HCV-replicating cells.

In contrast to our observations, it has been reported that the induction of CXC chemokines, particularly I-TAC, was significantly enhanced in HCV-replicating cells following stimulation with either IFN-γ or TNF-α and that stimulation with both had a synergistic effect (14). Although we confirmed that the expression of all of the CXC chemokines was significantly induced by stimulation with IFN-γ alone and costimulation with TNF-α in the HCV replicon-harboring cells (Fig. 1E and data not shown), only IP-10 was induced by stimulation with PGN or HA, suggesting that IP-10 is produced in HCV-replicating cells in a ligand-specific manner. The synergistic increase of I-TAC by the activation of IRF3 through a dsRNA-dependent signaling pathway has also been reported (13); however, it is difficult to reconcile the selective increase of I-TAC production by the dsRNA-mediated innate immune response because of the inhibition of the signaling pathway by the HCV NS3/-4A protease (25). Our data indicated that IP-10 production induced by HA or PGN is dependent upon the TLR2–MyD88–NF-κB axis, suggesting that the activation of NF-κB upon stimulation with HA plays a crucial role in the IP-10 production in cells replicating HCV. Although both the IP-10 and I-TAC promoters contain the ISRE, an increase in IP-10 production from stimulation with HCV RNA (5′ untranslated region), poly(I·C), IFN-γ, or TNF-α was not observed (13). Among the CXC chemokines, only IP-10 has two NF-κB-binding elements in the promoter, and the activation of IP-10 by stimulation with HA was mainly regulated by NF-κB but not ISRE in cells replicating HCV (Fig. 5E). These results strongly supported our notion that the selective increase of IP-10 production by stimulation with HA is dominantly regulated by the activation of NF-κB in the HCV-replicating cells.

CD44 variants have been implicated in many biological processes, including hematopoiesis, chronic inflammation, and metastatic spread of cancer cells (10, 38), and are useful markers in the diagnosis and prognosis of the progression of human tumors (11, 15). In chronic HCV infection, HA has been shown to be involved in HCV pathogenesis, while the participation of the specific CD44 variants has not been studied yet. The CD44v8 to -v10 variants have been shown to directly associate with TLR2 through the cytoplasmic domain and negatively regulate the inflammatory response in macrophages and mouse embryonic fibroblasts (21). Furthermore, it has been shown that the expression of CD44 contributes to the suppression of TLR4-mediated inflammation through the induction of the negative regulator in alveolar and peritoneal macrophages (27). The expression of TLR and CD44 variants varies among cell types, and the expression pattern of the molecules might determine the inflammatory response in cells infected with HCV. Further studies are needed to clarify the involvement of each of the CD44 variants in the pathogenesis of HCV.

Intervention to reduce the expression of endogenous HA and to inhibit the interaction between CD44 and TLR2 may provide a novel therapeutic measure for CHC patients exhibiting no response to the current pharmaceutical intervention.

ACKNOWLEDGMENTS

We are grateful to H. Murase and M. Tomiyama for their secretarial work. We also thank U. Günthert for providing a plasmid.

This work was supported in part by grants-in-aid from the Ministry of Health, Labor, and Welfare (Research on Hepatitis), the Ministry of Education, Culture, Sports, Science, and Technology, and the Osaka University Global Center of Excellence Program.

REFERENCES

1. Abe T, et al. 2007. Hepatitis C virus nonstructural protein 5A modulates the toll-like receptor-MyD88-dependent signaling pathway in macrophage cell lines. J. Virol. 81:8953–8966.
2. Boisvert J, et al. 2003. Liver-infiltrating lymphocytes in end-stage hepatitis C virus: subsets, activation status, and chemokine receptor phenotypes. J. Hepatol. 38:67–75.
3. Butera D, et al. 2005. Plasma chemokine levels correlate with the outcome of antiviral therapy in patients with hepatitis C. Blood 106:1175–1182.
4. Casrouge A, et al. 2011. Evidence for an antagonist form of the chemokine CXCL10 in patients chronically infected with HCV. J. Clin. Invest. 121:308–317.
5. Diago M, et al. 2006. Association of pretreatment serum interferon gamma inducible protein 10 levels with sustained virological response to peginterferon plus ribavirin therapy in genotype 1 infected patients with chronic hepatitis C. Gut 55:374–379.
6. Dolganiuc A, et al. 2003. Hepatitis C virus core and nonstructural protein 3 proteins induce pro- and anti-inflammatory cytokines and inhibit dendritic cell differentiation. J. Immunol. 170:5615–5624.
7. Dolganiuc A, et al. 2004. Hepatitis C core and nonstructural 3 proteins trigger Toll-like receptor 2-mediated pathways and inflammatory activation. Gastroenterology 127:1513–1524.
8. Ebihara T, Shingai M, Matsumoto M, Wakita T, Seya T. 2008. Hepatitis C virus-infected hepatocytes extrinsically modulate dendritic cell maturation to activate T cells and natural killer cells. Hepatology 48:48–58.
9. Guechot J, et al. 2000. Prognostic value of serum hyaluronan in patients with compensated HCV cirrhosis. J. Hepatol. 32:447–452.
10. Günthert U, et al. 1998. Functional involvement of CD44, a family of cell adhesion molecules, in immune responses, tumour progression and haematopoiesis. Adv. Exp. Med. Biol. 451:43–49.
11. Günthert U, et al. 1995. Are CD44 variant isoforms involved in human tumour progression? Cancer Surv. 24:19–42.
12. Harvey CE, et al. 2003. Expression of the chemokine IP-10 (CXCL10) by hepatocytes in chronic hepatitis C virus infection correlates with histological severity and lobular inflammation. J. Leukoc. Biol. 74:360–369.
13. Helbig KJ, et al. 2009. Differential expression of the CXCR3 ligands in chronic hepatitis C virus (HCV) infection and their modulation by HCV in vitro. J. Virol. 83:836–846.
14. Helbig KJ, et al. 2004. Expression of the CXCR3 ligand I-TAC by hepatocytes in chronic hepatitis C and its correlation with hepatic inflammation. Hepatology 39:1220–1229.
15. Herrlich P, et al. 1998. How tumor cells make use of CD44. Cell. Adhes. Commun. 6:141–147.
16. Heydtmann M, Adams DH. 2009. Chemokines in the immunopathogenesis of hepatitis C infection. Hepatology 49:676–688.
17. Itoh Y, et al. 2001. Clinical significance of elevated serum interferon-inducible protein-10 levels in hepatitis C virus carriers with persistently normal serum transaminase levels. J. Viral. Hepat. 8:341–348.
18. Jiang D, et al. 2005. Regulation of lung injury and repair by Toll-like receptors and hyaluronan. Nat. Med. 11:1173–1179.
19. Jiang D, Liang J, Noble PW. 2007. Hyaluronan in tissue injury and repair. Annu. Rev. Cell Dev. Biol. 23:435–461.
20. Kaimori A, et al. 2004. Pseudotype hepatitis C virus enters immature myeloid dendritic cells through the interaction with lectin. Virology 324:74–83.
21. Kawana H, et al. 2008. CD44 suppresses TLR-mediated inflammation. J. Immunol. 180:4235–4245.
22. Lagging M, et al. 2006. IP-10 predicts viral response and therapeutic outcome in difficult-to-treat patients with HCV genotype 1 infection. Hepatology 44:1617–1625.
23. Larrubia JR, Benito-Martinez S, Calvino M, Sanz-de-Villalobos E, Parra-Cid T. 2008. Role of chemokines and their receptors in viral persistence and liver damage during chronic hepatitis C virus infection. World J. Gastroenterol. 14:7149–7159.
24. Larrubia JR, et al. 2007. The role of CCR5/CXCR3 expressing CD8+ cells in liver damage and viral control during persistent hepatitis C virus infection. J. Hepatol. 47:632–641.
25. Lemon SM. 2010. Induction and evasion of innate antiviral responses by hepatitis C virus. J. Biol. Chem. 285:22741–22747.
26. Leroy V, et al. 2003. Phenotypic and functional characterization of intrahepatic T lymphocytes during chronic hepatitis C. Hepatology 38:829–841.
27. Liang J, et al. 2007. CD44 is a negative regulator of acute pulmonary inflammation and lipopolysaccharide-TLR signaling in mouse macrophages. J. Immunol. 178:2469–2475.
28. Lohmann V, et al. 1999. Replication of subgenomic hepatitis C virus RNAs in a hepatoma cell line. Science 285:110–113.
29. Marukian S, et al. 2008. Cell culture-produced hepatitis C virus does not infect peripheral blood mononuclear cells. Hepatology 48:1843–1850.
30. McHutchison JG, et al. 2000. Measurement of serum hyaluronic acid in patients with chronic hepatitis C and its relationship to liver histology. Consensus Interferon Study Group. J. Gastroenterol. Hepatol. 15:945–951.
31. Mielgo A, van Driel M, Bloem A, Landmann L, Günthert U. 2006. A novel antiapoptotic mechanism based on interference of Fas signaling by CD44 variant isoforms. Cell Death Differ. 13:465–477.
32. Moriishi K, Matsuura Y. 2003. Mechanisms of hepatitis C virus infection. Antivir. Chem. Chemother. 14:285–297.
33. Narumi S, et al. 1997. Expression of IFN-inducible protein-10 in chronic hepatitis. J. Immunol. 158:5536–5544.
34. Okamoto T, et al. 2008. A single-amino-acid mutation in hepatitis C virus NS5A disrupting FKBP8 interaction impairs viral replication. J. Virol. 82:3480–3489.
35. Patel K, et al. 2003. Clinical use of hyaluronic acid as a predictor of fibrosis change in hepatitis C. J. Gastroenterol. Hepatol. 18:253–257.
36. Patzwahl R, Meier V, Ramadori G, Mihm S. 2001. Enhanced expression of interferon-regulated genes in the liver of patients with chronic hepatitis C virus infection: detection by suppression-subtractive hybridization. J. Virol. 75:1332–1338.
37. Polyak SJ, Khabar KS, Rezeiq M, Gretch DR. 2001. Elevated levels of interleukin-8 in serum are associated with hepatitis C virus infection and resistance to interferon therapy. J. Virol. 75:6209–6211.
38. Ponta H, Sherman L, Herrlich PA. 2003. CD44: from adhesion molecules to signalling regulators. Nat. Rev. Mol. Cell Biol. 4:33–45.
39. Radkowski M, et al. 2004. Infection of primary human macrophages with hepatitis C virus in vitro: induction of tumour necrosis factor-alpha and interleukin 8. J. Gen. Virol. 85:47–59.
40. Romero AI, et al. 2006. Interferon (IFN)-gamma-inducible protein-10: association with histological results, viral kinetics, and outcome during treatment with pegylated IFN-alpha 2a and ribavirin for chronic hepatitis C virus infection. J. Infect. Dis. 194:895–903.
41. Scheibner KA, et al. 2006. Hyaluronan fragments act as an endogenous danger signal by engaging TLR2. J. Immunol. 177:1272–1281.
42. Shields PL, et al. 1999. Chemokine and chemokine receptor interactions provide a mechanism for selective T cell recruitment to specific liver compartments within hepatitis C-infected liver. J. Immunol. 163:6236–6243.
43. Shiina M, Rehermann B. 2008. Cell culture-produced hepatitis C virus impairs plasmacytoid dendritic cell function. Hepatology 47:385–395.
44. Takeuchi O, Akira S. 2010. Pattern recognition receptors and inflammation. Cell 140:805–820.
45. Ueno T, et al. 1995. Serum hyaluronate predicts response to interferon-alpha therapy in patients with chronic hepatitis C. Hepatogastroenterology 42:522–527.
46. Wakita T, et al. 2005. Production of infectious hepatitis C virus in tissue culture from a cloned viral genome. Nat. Med. 11:791–796.
47. Wang J, Holmes TH, Cheung R, Greenberg HB, He XS. 2004. Expression of chemokine receptors on intrahepatic and peripheral lymphocytes in chronic hepatitis C infection: its relationship to liver inflammation. J. Infect. Dis. 190:989–997.
48. Wong VS, et al. 1998. Serum hyaluronic acid is a useful marker of liver fibrosis in chronic hepatitis C virus infection. J. Viral Hepat. 5:187–192.
49. Zeremski M, et al. 2008. Intrahepatic levels of CXCR3-associated chemokines correlate with liver inflammation and fibrosis in chronic hepatitis C. Hepatology 48:1440–1450.

CLINICAL AND TRANSLATIONAL RESEARCH

V5-Drainage-Preserved Right Lobe Grafts Improve Graft Congestion for Living Donor Liver Transplantation

Takeo Toshima, Akinobu Taketomi, Toru Ikegami, Takasuke Fukuhara, Hiroto Kayashima, Tomoharu Yoshizumi, Yuji Soejima, Ken Shirabe, and Yoshihiko Maehara

Background. Right lobe (RL) grafts without middle hepatic vein for living donor liver transplantation (LDLT) result in congestion of recipients' livers and sometimes in unfavorable postoperative course. This study aimed to evaluate the feasibility of our new V5-drainage-preserved RL (VP-RL) graft.

Methods. Based on a review of 49 donors' livers in a retrospective study using three-dimensional reconstruction-computed tomography volumetry, hepatic vein draining segment 4 (V4) anatomy was classified into three types: inferior V4 dominant (A); superior V4 dominant (B); and umbilical vein to left hepatic vein dominant (C). Differences in functional graft volume (GV) and remnant liver volume (RV) between VP-RL and modified RL (M-RL) grafts with all three types were evaluated. In a prospective study of actual 15 LDLT, the outcome of venous reconstruction and postoperative parameters with VP-RL grafts compared with M-RL grafts was analyzed.

Results. In the retrospective study using three-dimensional reconstruction-computed tomography volumetry, in types B and C, functional GV of VP-RL was larger than that of M-RL ($P<0.05$) without impaired donors' functional RV, whereas functional RV in VP-RL was significantly decreased in type A ($P<0.05$). In the prospective study of actual 15 LDLT, using VP-RL with types B and C, size and number of venous reconstructions, and functional GV and postoperative parameters, such as postoperative serum total bilirubin levels and ascites volume, were significantly improved compared with those using M-RL ($P<0.05$).

Conclusions. Using preoperative V4 anatomical classification, VP-RL graft procurement is a valuable strategy in RL-LDLT to improve postoperative course of both recipients and donors.

Keywords: Liver transplantation, Graft congestion, Right lobe, Modified right lobe.

(*Transplantation* 2012;93: 929–935)

Living donor liver transplantation (LDLT) has become a potent treatment modality for end-stage liver disease since the first clinical report in 1989 (*1*). With the increase in adult LDLT cases, the procured graft volume (GV) has increased from a lateral segment to the left lobe, and even to the right lobe (RL), for adult LDLT (*2*). In LDLT using a RL, RL grafts without the middle hepatic vein (MHV) are usually donated to insure donor safety in our institute (*3, 4*). Despite favorable RL GV, complications such as a slow recovery of liver function and small-for-size syndrome, which is characterized by synthetic dysfunction, prolonged cholestasis, and persistent ascites, are sometimes present in recipients after LDLT (*5–9*). To resolve these problem, our previous study, using a three-dimensional reconstruction (3DR) of a computed tomography (CT) scan, demonstrated that reconstruction of the MHV tributaries, including the hepatic vein draining segment 5 (V5) and the hepatic vein draining segment 8 of the liver, is essential to avoid congestion of the anterior segment of the RL graft if the calculated area of congestion is more than 20% (*10*).

Since Lee et al. (*11*) first suggested the modified RL (M-RL) graft in 2002, many types of autogenous interposition vein grafts have been used, and we devised an explanted portal vein graft to effectively reconstruct MHV tributaries (*9*). Graft congestion, caused by thin MHV tributaries less than 5 mm, is almost compensated for by the formation of intrahepatic collaterals; however, a congested graft might sometimes cause impaired liver function when the

The authors declare no funding or conflicts of interest.

Department of Surgery and Science, Graduate School of Medical Sciences, Kyushu University, Fukuoka, Japan.

Address correspondence to: Akinobu Taketomi, M.D., Department of Surgery and Science, Graduate School of Medicine, Kyushu University, 3-1-1 Maidashi, Higashi-ku, Fukuoka 812-8582, Japan.

E-mail: taketomi@surg2.med.kyushu-u.ac.jp.

T.T. participated in the writing of the manuscript, research design, and data analysis; A.T. and Y.M. contributed to the discussion and reviewed the manuscript; T.I., T.Y., Y.S., and K.S. participated in research design; and T.F. and H.K. participated in the collecting the data.

Supplemental digital content (SDC) is available for this article. Direct URL citations appear in the printed text, and links to the digital files are provided in the HTML text of this article on the journal's Web site (www.transplantjournal.com).

Received 11 October 2011. Revision requested 27 October 2011.

Accepted 26 December 2011.

Copyright © 2012 by Lippincott Williams & Wilkins

ISSN: 0041-1337/12/9309–929

DOI: 10.1097/TP.0b013e3182488bd8

congestion is large (*10, 12*). To overcome this problem, an extended RL graft with the MHV is used in many countries; however, the donor's remnant liver tends to be small (*13, 14*). To maintain the volume of remnant liver volume (RV), Chan et al. (*15*) and Hwang et al. (*16*) demonstrated the feasibility of RL grafts with only the caudal MHV, which might lead to the donor's remnant liver with cranial MHV preserving hepatic vein draining segment 4 (V4) drainage.

On the basis of the strategy by Chan et al. (*15*), we devised a new concept to increase functional GV by improving congested volume (CV) in a procured RL graft with reconstruction of a large caudal MHV trunk draining all V5 tributaries. To select the appropriate liver type for our V5-drainage-preserved RL (VP-RL) graft, donor's livers were classified into three types by V4 anatomy. Furthermore, intraoperative venous reconstruction data and postoperative clinical parameters between VP-RL grafts and M-RL grafts were prospectively evaluated.

RESULTS

Classification of V4 Anatomy in the Retrospective Study

The anatomical patterns of V4 in 49 cases were as follows: type A, n=26; type B, n=15; and type C, n=8 (Fig. 1). Inferior V4 (V4 inf.) drainage territory in type A occupied 48.3%±13.2% of segment 4 of the liver (S4) volume, 19.4%±6.1% of left lobe volume, and 7.0%±2.0 % of whole liver volume (WLV). Superior V4 (V4 sup.) drainage territory in type B occupied 47.2%±12.4% of S4 volume, 19.0%±6.4% of left lobe, and 6.9%±1.8% of WLV. Umbilical vein (UV) from left hepatic vein (LHV) drainage territory in type C occupied 42.6%±12.2% of S4 volume, 17.1%±5.8% of left lobe volume, and 6.2%±1.4% of WLV.

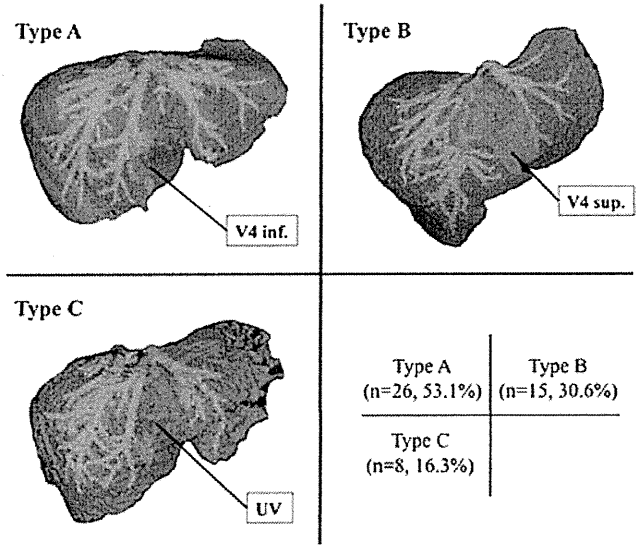

FIGURE 1. 3DR-CT images for classification of V4 anatomy in the retrospective study. The V4 anatomical patterns in 49 cases were classified into three types: A, B, and C, in which V4 inf., V4 sup., and UV from LHV predominantly drain, respectively. 3DR, three-dimensional reconstruction; CT, computed tomography; LHV, left hepatic vein; V4 inf., inferior V4; V4 sup., superior V4; UV, umbilical vein V4; V4, hepatic vein draining segment 4.

TABLE 1. Functional GV and RV with both M-RL and VP-RL grafts in all the V4 anatomical types in the retrospective study (n=49)

V4 classification	Functional GV (mL) (/WLV; %)	Functional RV (mL) (/WLV; %)
Type A (n=26)		
M-RL	593±28	368±16
	(59±2)	(36±2)
VP-RL	614±27	324±23
	(62±3)	(32±2)
P value	<0.05	<0.05
Type B (n=15)		
M-RL	619±34	362±19
	(60±2)	(35±1)
VP-RL	648±34	350±28
	(63±3)	(34±1)
P value	<0.05	NS
Type C (n=8)		
M-RL	642±45	370±25
	(58±3)	(36±2)
VP-RL	683±44	354±38
	(62±3)	(35±3)
P value	<0.05	NS

Values are mean±SD.

SD, standard deviation; M-RL, modified right lobe; GV, graft volume; LV, liver volume; NS, not significant; RL, right lobe; RV, remnant liver volume; VP-RL, V5-drainage-preserved right lobe; WLV, whole liver volume.

Simulation of M-RL and VP-RL Grafts With Three Types of V4 Anatomy in the Retrospective Study

Liver volume, such as GV and RV, was calculated by 3DR-CT volumetry. Functional GV and RV according to the donor's liver type are presented in Table 1. With type A, functional GV in the VP-RL graft was significantly higher than that in the M-RL graft ($P<0.05$); however, functional RV in the VP-RL graft was significantly lower than that in the M-RL graft ($P<0.05$). With types B and C, functional GV in the VP-RL graft was significantly higher than that in the M-RL graft ($P<0.05$), and functional RV in the VP-RL graft was similar to that in the M-RL graft. Considering donor safety, the criteria for graft selection in the prospective study were VP-RL with types B and C, whereas for the M-RL graft, only type A was used.

Outcome of 3DR-CT Volumetry and Venous Reconstruction in the Prospective Study

Baseline characteristics in both donors and recipients were not significantly different between the two groups (data not shown). The data of 3DR-CT volumetry and venous reconstruction are presented in Table 2. For the outcome of donors' side, any parameters, such as WLV and RV, were not significantly different between the groups. Meanwhile, for the outcome of recipients' side, there were no significant

© 2012 Lippincott Williams & Wilkins

TABLE 2. Outcome of 3DR-CT volumetry, venous reconstruction, and postoperative clinical parameters in the prospective study

Variables	M-RL group (n=7)	VP-RL group (n=8)	*P*
3DR-CT volumetry			
WLV (mL)	986±41	1015±38	NS
RV (mL)	364±14	359±13	NS
Functional RV (mL)	364±15	330±14	NS
GV (mL)	622±32	656±30	NS
SLV (mL)	1191±47	1284±44	NS
GRWR (%)	1 .00±0.18	0.95±0.33	NS
GV/SLV (%)	52.2±7.2	52.4±14.6	NS
CV (mL)	91±13	47±13	<0.05
CV/GV (%)	9.4±1.4	4.6±1.3	<0.05
Functional GV (mL)	531±37	609±35	<0.05
Venous reconstruction			
Mean size of MHV trunk or V5 (mm)	6.6±0.8	11.4±0.7	<0.01
Proportion of grafts with MHV trunk or V5<10 mm in diameter (%)	6 (85.7)	1 (12.5)	<0.01
Number of MHV trunks or V5	2.9±0.2	1.0±0.2	<0.01
Postoperative parameters of donors			
Operative time (min)	419±16	428±15	NS
Operative blood loss (g)	346±60	420±57	NS
Peak serum T-Bil levels (mg/dL)	2.4±0.3	3.0±0.2	NS
Peak serum ALT levels (U/L)	725±114	531±107	NS
Hospital stay (d)	16±1	13±1	NS
Complications greater than Clavien grade 1 (%)	2 (28.6)	1 (12.5)	NS
Postoperative parameters of recipients			
Operative time (min)	908±34	861±31	NS
Operative blood loss (g)	5349±1402	4524±1312	NS
Hospital stay (d)	36±7	26±7	NS
Complications greater than Clavien grade 3 (%)	2 (28.6)	2 (25.0)	NS
Serum T-Bil levels (mg/dL)			
POD 1	9.4±5.5	4.6±1.2	<0.05
POD 3	4.8±2.4	2.7±0.6	<0.05
POD 5	7.8±4.1	5.4±1.4	NS
POD 7	6.1±4.3	3.2±2.6	NS
Ascites volume on POD 7 (mL)	431±254	59±83	<0.01
Duration of postoperative drainage (d)	16±10	7±2	<0.05

Means are given as±SD or n (%).

3DR-CT, three-dimensional reconstruction-computed tomography; ALT, alanine aminotransferase; CV, congestive volume; GRWR, graft recipient's body weight ratio; GV/SLV, graft volume to recipient standard liver volume ratio; MHV, middle hepatic vein; M-RL, modified right lobe; NS, not significant; POD, postoperative day; RV, remnant liver volume; SLV, standard liver volume; T-Bil, total bilirubin; VP-RL, V5-drainage-preserved right lobe; WLV, whole liver volume.

differences in the graft recipient's body weight ratio and GV versus standard liver volume ratio between the groups. However, CV and CV/GV in the VP-RL graft were significantly lower than those in the M-RL graft ($P<0.05$); therefore, functional GV in the VP-RL graft was significantly higher than that in the M-RL graft ($P<0.05$). With respect to intraoperative venous reconstruction, the mean size of the MHV trunk in the VP-RL graft was significantly larger than that of V5 branches in the M-RL graft ($P<0.01$), and the rate of grafts with MHV less than 10 mm in diameter and the number of MHV trunks in the VP-RL graft were significantly lower than those of V5 branches in the M-RL graft ($P<0.01$).

Comparison of Postoperative Clinical Parameters in the Prospective Study

The clinical parameters in donors, such as operative time, operative blood loss, peak values of liver function tests, and incidence of complications are presented in Table 2. There were no significant differences in these parameters between the groups. For the clinical parameters of recipients, with respect to baseline characteristics of graft hemodynamics,

there were no significant differences in portal vein pressure after laparotomy and before abdominal closure, and in the prevalence of refractory ascites, gastrointestinal bleeding, spontaneous splenorenal shunt, transjuglar intrahepatic portosystemic shunt, splenectomy, and ligation of the shunt between M-RL and VP-RL grafts (see **Table, SDC 1,** http://links.lww.com/TP/A641). Data such as operative time, operative blood loss, and hospital stay were not significantly different between the groups (Table 2). The ratio of complications greater than Clavien grade 3 was comparable between the groups: pancreas pseudoaneurysm and intraperitoneal abscess (n = 1) and partial thrombus of the portal vein trunk (n = 1) were found in VP-RL grafts, and thrombus of the portal vein trunk requiring abdominal surgery (n = 1) and bile duct stenosis (n = 1) were found in M-RL grafts (Table 2). Serum total bilirubin (T-Bil) values at postoperative days 1 and 3 in VP-RL grafts were significantly lower than those in M-RL grafts ($P<0.05$) (Table 2). Other function tests such as serum aspartate aminotransferase (AST), alanine aminotransferase (ALT), and prothrombin time were not significantly different between the two groups (data not shown). Ascites volume at postoperative day 7 and the duration of postoperative drainage in VP-RL grafts were significantly lower than those in M-RL grafts (ascites volume, $P<0.01$; duration of postoperative drainage, $P<0.05$) (Table 2). All the grafts and patients survived in the prospective study, including both donors and recipients (the mean follow-up time was 32.7 months).

DISCUSSION

On the basis of the study by Chan et al., tailoring the donation of extended RL (*15*), we classified V4 anatomy in more detail to select an appropriate donor liver type for VP-RL grafts. From our study results, we concluded that VP-RL grafts have a more favorable outcome compared with M-RL grafts. Moreover, types B and C, in which V4 sup. and the UV from LHV predominantly drain S4, were appropriate for VP-RL grafts because of their stable functional RV (Table 1). This could be a strategy against a slow postoperative recovery of liver function or small-for-size syndrome for complications in the recipient. In addition, by using VP-RL grafts with liver types B and C, the size and number of venous reconstructions, and functional GV were significantly improved compared with those using M-RL grafts. Furthermore, postoperative clinical parameters such as ascites volume and serum T-Bil values in VP-RL grafts were significantly improved.

One of the crucial problems for using RL grafts without the MHV is liver dysfunction caused by deficiency of GV or excessive CV (*5, 7*). There are some reports regarding the impact of liver congestion (*7, 10–12, 17–19*). Maetani et al.

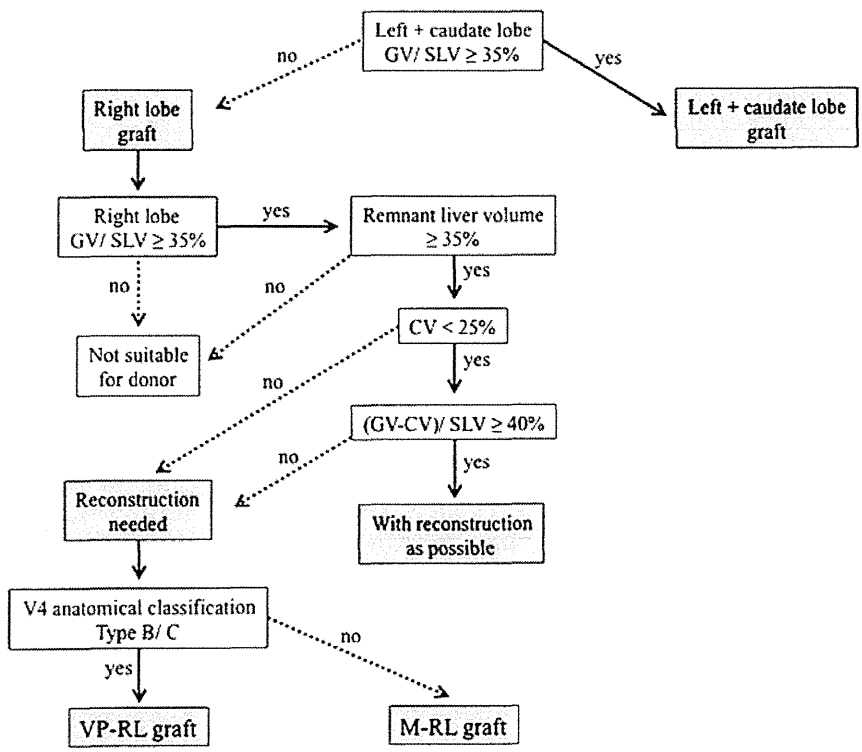

FIGURE 2. Algorithm for the graft selection as used in our institution. The RL graft is chosen if the estimated extended left with caudate lobe volume is less than 35% of the recipient's SLV. If a RV after procurement is less than 35% of WLV, this donor should be rejected. If CV is more than 25% or the deducted CV from the GV is less than 40% of the recipient's SLV, reconstruction of these tributaries is required. If the donor's liver is type B or C by V4 anatomical classification, a VP-RL graft is procured, whereas with type A, a M-RL graft is procured. SLV, standard liver volume; CV, congested volume; GV, graft volume; RV, remnant liver volume; M-RL, modified right lobe, RL, right lobe; VP-RL, V5-drainage-preserved right lobe; WLV, whole liver volume; V4, hepatic vein draining segment 4.

© 2012 Lippincott Williams & Wilkins

(*17*) demonstrated that for a long-term outcome of 6 postoperative months, the lack of anterior segment regeneration was resolved by a compensatory regeneration of the posterior segment and graft congestion in the anterior segment did not affect overall graft regeneration. On the other hand, for the short-term outcome as postoperative 7 days when postoperative complications sometimes occur, we previously demonstrated that congestion of the anterior segment caused by impaired outflow was severe in several cases, and sometimes the estimated CV exceeded 50% of the RL volume (*7, 10, 12*). This graft congestion could lead to transient liver dysfunction and poor regeneration during the early postoperative period. In addition, Akamatsu et al. (*18*) and Mizuno et al. (*19*) demonstrated that liver regeneration in the congestion area is significantly poorer compared with that in the noncongestion area. Therefore, even in LDLT using RL grafts where the actual GV may be relatively large, the impact of congestion cannot be ignored. Regarding the benefit with reconstruction of MHV tributaries, at least in the short-term, we observed some favorable outcomes such as an improvement in serum T-Bil levels and ascites volume by reducing congestion of the anterior segment in VP-RL grafts.

The advantage of VP-RL grafts was that there was no CV of S5 in the recipient liver, but there was minimal CV of S4 in the donor liver. Considering donor safety, type A could not be used for the VP-RL graft because functional RV in the VP-RL graft was significantly lower than that in the M-RL graft with type A (Table 1). Based on these findings, an algorithm for graft selection was determined (Fig. 2). The left lobe is initially considered as a graft with respect to donor safety. The RL graft is chosen if the estimated extended left with caudate lobe volume is less than 35% of the recipient's standard liver volume (SLV). If a RV after RL procurement is less than 35% of WLV, this donor should be rejected. If CV is more than 25% or the deducted CV from the GV is less than 40% of the recipient's SLV, reconstruction of these tributaries is required. If the donor's liver is type B or C by V4 anatomical classification, a VP-RL graft is procured, whereas with type A, a M-RL graft is procured.

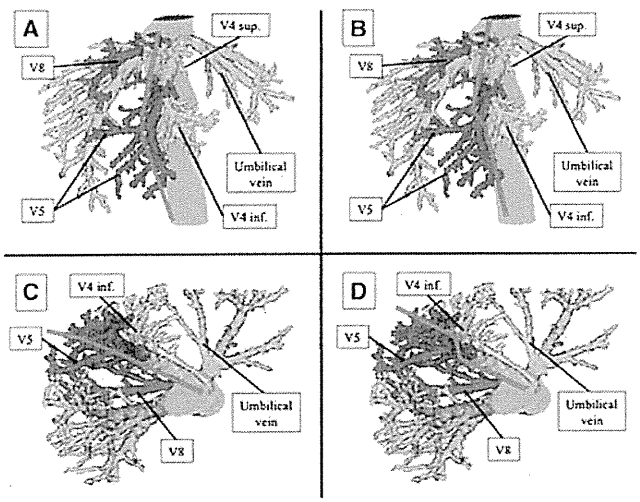

FIGURE 3. Stereoscopic images by 3DR-CT for transection lines in both M-RL and VP-RL grafts. Representative images of a M-RL graft where the transection line is along the right side of the MHV in a coronal plane image (A) and sagittal plane image (C). There is likely to be mild CV of the anterior segment in the recipient liver but no CV of S4 in the donor liver. Representative images of a VP-RL graft where the transection line is along the left side of the caudal MHV and is cut off the caudal MHV trunk and the right side of the cranial MHV in a coronal plane image (B) and sagittal plane image (D). There is not likely to be CV of S5 in the recipient liver with caudal MHV trunk reconstruction, but there might be a little CV of S4 in the donor liver. 3DR, three-dimensional reconstruction; CT, computed tomography; CV, congested volume; MHV, middle hepatic vein; M-RL, modified right lobe, RL, right lobe; S4, segment 4; S5, segment 5; S8, segment 8; VP-RL, V5-drainage-preserved right lobe; V4 inf., inferior V4; V4 sup., superior V4.

Since the M-RL graft was first demonstrated by Lee et al. (*11*), there have been some reports demonstrating the reconstruction method of V5 and hepatic vein draining segment 8 to prevent congestion of the anterior segment. We previously demonstrated the feasibility of autogenous interposition vein grafts, such as the portal vein, saphenous vein, inferior vena cava, inferior mesenteric vein, and internal jugular vein (*8, 9*). Another method to improve CV is to use an extended RL graft with the whole MHV (*13, 14*). To overcome CV of S4 in the donor's remnant liver, Chan et al. (*15*) procured an extended RL with only the caudal MHV. With this particular graft, the donors' postoperative clinical parameters were significantly improved compared with normal extended RL; however, their strategy has a major limitation. It was not clear how the V4 anatomical classification by which the donor's liver type their tailoring extended RL should be procured. They also classified V4 anatomy into three types based on S4 drainage into the MHV, UV, and equally into MHV and UV. However, in our retrospective analysis, functional RV was significantly decreased in LDLT using the VP-RL graft with type A in which V4 inf. predominantly drains S4. Furthermore, the cutoff level of the MHV trunk needed be clear, immediately above the MHV where all V5 drains into, to preserve the thick caudal MHV trunk to reconstruct for complete drainage of S5.

In conclusion, VP-RL graft procurement is a safe and reliable RL graft for improving functional LV and the postoperative clinical course in the recipients, without impairment of functional RV and the postoperative clinical course in the donors by venous reconstruction with a large-sized caudal MHV. Using preoperative V4 anatomical graft classification, a suitable liver type of the donor for the VP-RL graft should be selected to ensure a good outcome for both recipients and donors. However, these data should be interpreted carefully because of the small numbers of cases, and step-by-step analysis is essential to strengthen the interpretation.

MATERIALS AND METHODS

Donors in the Retrospective Study and Patients in the Prospective Study

From July 2004 to May 2008, measurements of GV from preoperative 3DR-CT volumetry for LDLT using RL grafts at Kyushu University Hospital were retrospectively evaluated for 49 donors. The characteristics and 3DR-CT volumetry of the 49 donors were as follows: age, 35 years; proportion of males, 65.3%; height, 167 cm; weight, 61 kg; body mass index,

22.3 mg/dL; serum T-Bil, 0.6 mg/dL; serum AST, 17 U/L; ALT, 17 U/L; WLV, 913 mL; GV, 520 mL; and RV, 393 mL.

Patients in the Prospective Study

For the prospective study, 15 donors were evaluated from June 2008 to February 2009. The characteristics and 3DR-CT volumetry of the 15 donors were as follows: age, 37 years; proportion of males, 40.0%; height, 162 cm; weight, 56 kg; body mass index, 21.6 mg/dL; serum T-Bil, 0.6 mg/dL; serum AST, 20 U/L; ALT, 19 U/L; WLV, 1002 mL; GV, 640 mL; and RV, 361 mL. None of these parameters in the 15 donors in the prospective study were significantly different from those in the 49 donors in the retrospective study (data not shown).

The indications for LDLT in the prospective study were liver cirrhosis resulting from unknown cause (n = 3), hepatitis C (n = 7), hepatitis B (n = 2), alcohol abuse (n = 1), Wilson disease (n = 1), and chronic rejection (n = 1). Eight patients had liver cirrhosis with hepatocellular carcinoma. All LDLTs were performed after obtaining full informed consents from all patients and approval by the Liver Transplantation Committee of Kyushu University. The study protocol confirmed to the ethical guidelines of the 1975 Helsinki Declaration and was approved by our institutional review board.

Graft Selection and Criteria for Venous Reconstruction

Graft selection, including reconstruction of the MHV tributaries, was performed according to a previously described algorithm (*10*). The SLV of recipients was calculated according to the formula described by Urata et al. (*20*). The explanted portal vein grafts were used for the reconstruction of MHV tributaries in 10 cases, and other interposition grafts included the saphenous vein (n = 4), inferior mesenteric vein (n = 3), and internal jugular vein (n = 3).

Classification of V4 Anatomy and Evaluation of Functional GV and RV

LV, CV, and drainage volume of each small vein were calculated by specialized computer software (Resion Growing Software Version 0.5a; Hitachi Medical Corporation, Chiba, Japan). By using this software, the stereoscopic patterns of V4 were visualized through 3DR of preoperative dynamic CT images. Additionally, based on their diameter and length, WLV and the volume of each hepatic venous branch territory were automatically calculated (*10, 12, 21*). To identify the predominant V4 branch for S4, we calculated a drainage liver volume for each of the V4 branches. The CV/WLV ratio for each of the V4 branches was also calculated. Based on these evaluated data, V4 anatomical patterns were then classified into three groups as types A, B, and C, which predominantly drain S4 as the V4 inf., the V4 sup., or the UV to LHV, respectively (Fig. 1). Both M-RL and VP-RL grafts were retrospectively simulated with all three types to calculate the functional GV and the functional RV by deducting CV, which was computed by the sum of the venous branches that were not reconstructed (*10, 12*).

Surgical Procedure With M-RL graft and VP-RL Graft Donation

Figure 3 shows stereoscopic images through 3DR-CT images with simulated different patterns for the two types of transection lines, for the M-RL graft (Fig. 3A) and VP-RL graft (Fig. 3B) in the donated liver. The operative procedures with M-RL grafts have been described elsewhere (*3, 4, 22, 23*). Significant drainage veins from the anterior segment and inferior right hepatic veins more than 5 mm in diameter were clipped and procured with grafts for reconstruction at the back table. There was mild CV of the anterior segment in the recipient liver but no CV of S4 in the donor liver because the numbers of V5 were not always simple and the interposition grafts to be anastomosed with the RHV were limited in number.

The VP-RL graft was procured by transecting along the left side of the caudal MHV, it was cut off the caudal MHV trunk, and then transected along the right side of the following cranial MHV, as described previously (*15*) (Fig. 3B). To preserve the thick caudal MHV trunk with the graft and to reconstruct for complete drainage of S5, the MHV trunk was transected immediately above the MHV where all V5 drained into. There was no CV of S5 in the recipient liver, but there was a little CV of S4 in the donor liver. The size and number of V5 branches in the M-RL graft were measured and those of the MHV trunk in the VP-RL graft.

Evaluation of Postoperative Clinical Parameters in the Prospective Study

After preoperative V4 classification through 3DR-CT images, M-RL grafts were procured in donors with type A of the V4 anatomical classification, and VP-RL grafts were procured in those with types B and C. The clinical follow-up of patients after LDLTs followed a strict protocol, which did not change during the study period (*3, 4*). The operative time and intraoperative blood loss were measured, and postoperative complications including ascites volume and hospital stay were compared between the two types of grafts. Complications were classified according to Clavien's classification (*24*). The indication to remove drains was when the postoperative drainage volume was less than 500 mL/day and the general condition of the patients including other laboratory data were improved. When the patients' condition was not improved or clinically stable, drains were not removed.

Statistical Analysis

All statistical analyses were performed using JMP statistical software version 7.01 (SAS Institute Inc., Cary, NC). All variables are expressed as the mean±standard deviation. The continuous variables were compared with independent samples using the nonparametric Wilcoxon test or with dependent samples using the parametric paired t test. The categorical data were compared using the Fisher's test and χ^2-squared test. P values less than 0.05 were considered significant.

ACKNOWLEDGMENT

The authors thank Ms. Natsumi Yamashita for her valuable expert advice on the statistical analysis.

REFERENCES

1. Raja S, Nery JR, Mies S. Liver transplantation from live donors. *Lancet* 1989; 2: 497.
2. Soejima Y, Taketomi A, Yoshizumi T, et al. Feasibility of left lobe living donor LT between adults: An 8-year, single-center experience of 107 cases. *Am J Transplant* 2006; 6: 1004.
3. Taketomi A, Morita K, Toshima T, et al. Living donor hepatectomies with procedures to prevent biliary complications. *J Am Coll Surg* 2010; 211: 456.
4. Taketomi A, Kayashima H, Soejima Y, et al. Donor risk in adult-to-adult living donor liver transplantation: Impact of left lobe graft. *Transplantation* 2009; 87: 445.
5. Lee S, Park K, Hwang S, et al. Congestion of right liver graft in living donor liver transplantation. *Transplantation* 2007; 71: 812.
6. Suehiro T, Shimada M, Kishikawa K, et al. Effect of intraportal infusion to improve small for size graft injury in living donor adult liver transplantation. *Transpl Int* 2005; 18: 923.
7. Sanefuji K, Iguchi T, Ueda S, et al. New prediction factors of small-for-size syndrome in living donor adult liver transplantation for chronic liver disease. *Transpl Int* 2009; 23: 350.
8. Soejima Y, Ueda N, Fukuhara T, et al. One-step venous reconstruction for a right lobe graft with multiple venous orifices in living donor liver transplantation. *Liver Transpl* 2008; 14: 706.
9. Ikegami T, Soejima Y, Taketomi A, et al. Explanted portal vein grafts for middle hepatic vein tributaries in living-donor liver transplantation. *Transplantation* 2007; 84: 836.
10. Yonemura Y, Taketomi A, Soejima Y, et al. Validity of preoperative volumetric analysis of congestion volume in living donor liver transplantation using three-dimensional computed tomography. *Liver Transpl* 2005; 11: 1556.
11. Gyu Lee S, Min Park K, Hwang S, et al. Modified right liver graft from a living donor to prevent congestion. *Transplantation* 2002; 74: 54.
12. Fukuhara T, Umeda K, Toshima T, et al. Congestion of the donor remnant right liver after extended left lobe donation. *Transpl Int* 2009; 22: 837–844.
13. Kasahara M, Takada Y, Fujimoto Y, et al. Impact of right lobe with middle hepatic vein graft in living-donor liver transplantation. *Am J Transplant* 2005; 5: 1339.

© 2012 Lippincott Williams & Wilkins

14. Liu CL, Fan ST, Lo CM, et al. Operative outcomes of adult-to adult right lobe live donor liver transplantation: A comparative study with cadaveric whole-graft liver transplantation in a single center. *Ann Surg* 2006; 243: 404.
15. Chan SC, Lo CM, Liu CL, et al. Tailoring donor hepatectomy per segment 4 venous drainage in right lobe live donor liver transplantation. *Liver Transpl* 2004; 10: 755.
16. Hwang S, Lee SG, Choi ST, et al. Hepatic vein anatomy of the medial segment for living donor liver transplantation using extended right lobe graft. *Liver Transpl* 2005; 11: 449.
17. Maetani Y, Itoh K, Egawa H, et al. Factors influencing liver regeneration following living-donor liver transplantation of the right hepatic lobe. *Transplantation* 2003; 75: 97.
18. Akamatsu N, Sugawara Y, Kaneko J, et al. Effects of middle hepatic vein reconstruction on right liver graft regeneration. *Transplantation* 2003; 76: 832.
19. Mizuno S, Iida T, Yagi S, et al. Impact of venous drainage on regeneration of the anterior segment of right living-related liver grafts. *Clin Transpl* 2006; 20: 509.
20. Urata K, Kawasaki S, Matsunami H, et al. Calculation of child and adult standard liver volume for liver transplantation. *Hepatology* 1995; 21: 1317.
21. Kayashima H, Taketomi A, Yonemura Y, et al. Accuracy of an age-adjusted formula in assessing the graft volume in living donor liver transplantation. *Liver Transpl* 2008; 14: 1366.
22. Imamura H, Takayama T, Sugawara Y, et al. Pringle's maneuver in living donors. *Lancet* 2002; 360: 2049.
23. Kokudo N, Imamura H, Sano K, et al. Ultrasonically assisted retrohepatic dissection for a liver hanging maneuver. *Ann Surg* 2005; 242: 651.
24. Dindo D, Demartines N, Clavien PA. Classification of surgical complications. A new proposal with evaluation in a cohort of 6336 patients and results of a survey. *Ann Surg* 2004; 240: 205.

eTOCs and Publish Ahead-of-Print (PAP) Alerts

Receive the latest developments in transplantation as soon as they're available. Request delivery of Transplantation's electronic **Table of Contents (eTOC) and Publish Ahead-of-Print (PAP) Alerts.**

These are fast, easy and free services to all. You will receive:

- Complete Table of Contents for all new issues.
- Notice of all Publish Ahead-of-Print articles as they are posted at the Transplantation website.

For eTOC, visit www.transplantjournal.com and click on eTOC, to subscribe via email.

For PAP alerts, go to http://journals.lww.com/transplantjournal/toc/publishahead and click to subscribe via email or RSS feed.

JVI Journals.ASM.org

Baculovirus GP64-Mediated Entry into Mammalian Cells

Chikako Kataoka,[a] Yuuki Kaname,[a]* Shuhei Taguwa,[a]* Takayuki Abe,[a]* Takasuke Fukuhara,[a] Hideki Tani,[b] Kohji Moriishi,[c] and Yoshiharu Matsuura[a]

Department of Molecular Virology, Research Institute for Microbial Diseases, Osaka University, Osaka,[a] Department of Virology I, National Institute of Infectious Diseases, Tokyo,[b] and Department of Microbiology, Faculty of Medicine, Yamanashi University, Yamanashi,[c] Japan

The baculovirus *Autographa californica* multiple nucleopolyhedrovirus (AcMNPV) serves as an efficient viral vector, not only for abundant gene expression in insect cells, but also for gene delivery into mammalian cells. Lentivirus vectors pseudotyped with the baculovirus envelope glycoprotein GP64 have been shown to acquire more potent gene transduction than those with vesicular stomatitis virus (VSV) envelope glycoprotein G. However, there are conflicting hypotheses about the molecular mechanisms of the entry of AcMNPV. Moreover, the mechanisms of the entry of pseudotyped viruses bearing GP64 into mammalian cells are not well characterized. Determination of the entry mechanisms of AcMNPV and the pseudotyped viruses bearing GP64 is important for future development of viral vectors that can deliver genes into mammalian cells with greater efficiency and specificity. In this study, we generated three pseudotyped VSVs, NPVpv, VSVpv, and MLVpv, bearing envelope proteins of AcMNPV, VSV, and murine leukemia virus, respectively. Depletion of membrane cholesterol by treatment with methyl-β-cyclodextrin, which removes cholesterol from cellular membranes, inhibited GP64-mediated internalization in a dose-dependent manner but did not inhibit attachment to the cell surface. Treatment of cells with inhibitors or the expression of dominant-negative mutants for dynamin- and clathrin-mediated endocytosis abrogated the internalization of AcMNPV and NPVpv into mammalian cells, whereas inhibition of caveolin-mediated endocytosis did not. Furthermore, inhibition of macropinocytosis reduced GP64-mediated internalization. These results suggest that cholesterol in the plasma membrane, dynamin- and clathrin-dependent endocytosis, and macropinocytosis play crucial roles in the entry of viruses bearing baculovirus GP64 into mammalian cells.

Viruses represent highly evolved natural vectors for the transfer of foreign genetic information into cells (74). This attribute has enabled the engineering of recombinant viral vectors based on retrovirus, lentivirus, adenovirus, adeno-associated virus, herpesvirus, and baculovirus for the delivery of the foreign genes into target tissues. While substantial progress has been made, further vector refinement is required to overcome cytotoxicity, the induction of host immune responses, and the expression of viral genes before such vectors can be approved for clinical use for any individual disorder.

Baculovirus is an insect virus possessing a large double-stranded circular DNA genome packaged into a rod-shaped capsid. Among the numerous baculoviruses, *Autographa californica* multiple nucleopolyhedrovirus (AcMNPV) is the species most frequently used for baculovirus studies. Although AcMNPV has long been used as an efficient gene expression vector in insect cells (41, 45), recombinant baculoviruses were shown to be capable of entering into various mammalian cells without any replication and of expressing foreign genes under the control of mammalian promoters (11, 17, 65, 70, 71). Therefore, baculovirus is now recognized as a useful viral vector, not only for abundant gene expression in insect cells, but also for gene delivery into mammalian cells. In addition to achieving efficient gene delivery, AcMNPV has also been shown to stimulate host antiviral immune responses in mammalian cell lines (1–3, 24, 33, 63, 73, 77) and to confer protection from lethal virus infection (3, 24) and progressive tumor metastasis in mice (33). Furthermore, baculovirus has been utilized as both a ubiquitous and a specific gene transfer vector in the form of a recombinant virus bearing foreign proteins on the viral surface in addition to GP64, which is the major envelope glycoprotein of AcMNPV (70, 71), and of a pseudotyped virus displaying ligands of interest alone without GP64 (32), respectively.

The mechanism of entry of AcMNPV has been studied mainly in insect cells by using the extracellular budded viruses. AcMNPV was shown to become internalized by receptor-mediated endocytosis (26, 49, 58), and GP64 is initially involved in virus attachment on the cell surface. In a recent study, heparan sulfate was shown to be essential for gene transduction by baculovirus into mammalian cells (78). After receptor-mediated internalization of AcMNPV (26), GP64 undergoes conformational change into a fusion-competent state at low pH, and the nucleocapsid is released into the cytoplasm after cell fusion (14, 43, 63, 73). Furthermore, GP64-null viruses exhibited approximately 98% reduction in viral budding (7), indicating that GP64 is involved, not only in viral entry, but also in the egress of viral particles from infected cells.

Although the mechanisms of entry of AcMNPV into not only insect cells, but also mammalian cells, have not been well characterized, previous reports suggested that AcMNPV enters cells

Received 1 November 2011 Accepted 9 December 2011
Published ahead of print 21 December 2011
Address correspondence to Yoshiharu Matsuura, matsuura@biken.osaka-u.ac.jp.
* Present address: Y. Kaname, London School of Hygiene and Tropical Medicine, London, United Kingdom; S. Taguwa, Department of Biology, James H. Clark Center, Stanford University, Stanford, California, USA; T. Abe, Department of Medicine, University of Miami School of Medicine, Miami, Florida, USA.
Copyright © 2012, American Society for Microbiology. All Rights Reserved.
doi:10.1128/JVI.06704-11

through a clathrin-dependent (40, 44) or -independent (36) endocytic pathway. Moreover, it was shown recently that AcMNPV enters cells through direct fusion with the plasma membrane at low pH (7, 19). We reported previously that the entry of AcMNPV into mammalian cells was inhibited by treatment with purified lipids and was reduced in mutant hamster cell lines deficient in phospholipid synthesis (71). Furthermore, we have shown that GP64 interacts with CD55/decay-accelerating factor (DAF) in a lipid raft and confers resistance to serum inactivation (30). These data suggest that GP64's interaction with phospholipids on the cell surface plays an important role in the internalization of AcMNPV into mammalian cells. The lipid raft is a cholesterol-rich microdomain on the cell surface. It is characterized by detergent insolubility; light density; enrichment of cholesterol, glycosphingolipids, and glycosylphosphatidylinositol-anchored protein; and participation in cell surface receptor-mediated signal transduction, protein sorting, and membrane transport (9, 66). The lipid raft has been shown to play an important role in the entry of vaccinia virus (15) and Ebola virus (4), and in not only the entry but also the budding of influenza virus (12, 60) and human immunodeficiency virus (HIV) (55).

In the present study, we investigated the mechanisms of GP64-mediated viral entry into mammalian cells by using vesicular stomatitis virus (VSV) pseudotyped particles bearing various viral envelope proteins, including GP64 of AcMNPV and a recombinant AcMNPV possessing a luciferase gene under the control of a mammalian promoter. Depletion of membrane cholesterol by methyl-β-cyclodextrin (MβCD) impaired GP64-mediated entry in a dose-dependent manner but did not affect attachment to the cell surface. Inhibition of the dynamin-, clathrin-, and macropinocytosis-mediated pathways by using inhibitors and dominant-negative mutants impaired GP64-mediated entry, whereas the inhibition of caveolin-mediated endocytosis had no such effect. These results suggest that cell surface cholesterol, dynamin- and clathrin-mediated endocytoses, and macropinocytosis participate in the internalization of viral particles bearing GP64 into mammalian cells.

MATERIALS AND METHODS

Cells. Sf9 cells derived from *Spodoptera frugiperda* were grown in SF900-II medium (Invitrogen, Carlsbad, CA) supplemented with or without 10% fetal bovine serum (FBS) (Sigma, St. Louis, MO) at 27°C. Huh7 and 293T cell lines were cultured in Dulbecco's modified Eagle's medium (DMEM) (Sigma) supplemented with 10% FBS.

Antibodies. Anti-GP64 monoclonal antibodies (AcV1 and AcV5) were obtained from Santa Cruz Biotechnology (Santa Cruz, CA). Rabbit anti-VP39 polyclonal antibody was prepared by intradermal injection of the synthetic peptides of amino acid residues 37 to 49 (SPDAYHDDGW FIC) of AcMNPV VP39 into a Japanese white rabbit purchased from Kitayama Laboratories (Nagano, Japan). Antibodies to caveolin-1, calreticulin, β-actin, and the FLAG tag (M2) were purchased from Sigma. Antibodies to the hemagglutinin (HA) tag and green fluorescent protein (GFP) were purchased from Covance (Richmond, CA) and Clontech, respectively.

Plasmids. The cDNA encoding AcMNPV GP64 was generated by PCR, cloned into pCAGGS/MCS-PM (56), and designated pCAGGP64. pCAGVSVG, a plasmid encoding VSV-G protein under the control of the CAG promoter, was constructed as described previously (69). HA-tagged dynamin 2 (Dyn2), a dominant-negative Dyn2 (K44A) in which lysine^{44} is replaced with alanine, FLAG-tagged epidermal growth factor (EGF) receptor substrate 15 (Eps15), a dominant-negative Eps15 (Δ95-295), Glu/Glu (EE)-tagged Rab34, and a dominant-negative Rab34 (T66N) in which threonine^{66} is replaced with asparagine were cloned into pcDNA3.1. Caveolin-1 (CAV1) and a dominant-negative mutant (CAV1^{DGV}) were cloned into pAcGFP-C1 (Clontech, Mountain View, CA) (61). pSilencer-CAV1, carrying a short hairpin RNA (shRNA) targeted to CAV1 under the control of the U6 promoter, was constructed by cloning of the oligonucleotide pair 5′-GATCCGATTGACTTTGAAGATGTGTTCAAGAGA CACATCTTCAAAGTCAATCTTTTTTGGAAA-3′ and 5′-AGCTTTTCCAAAAAAGATTGACTTTGAAGATGTGTCTCTTGAACA CATCTTCAAAGTCAATCG-3′ between the cloning sites of pSilencer 2.1-U6 hygro (Ambion, Austin, TX). The pSilencer negative-control plasmid (Ambion) has no homology to any human gene. The plasmids used in this study were confirmed by sequencing with ABI Prism genetic analyzer 3130 (Applied Biosystems, Tokyo, Japan).

Production of pseudotyped VSVs and recombinant AcMNPV. Pseudotyped VSVs and recombinant baculoviruses were generated as described previously (30). To generate pseudotyped VSVs bearing the GP64 protein of AcMNPV (NPVpv), the G protein of VSV (VSVpv), and the GP70 protein of murine leukemia virus (MLVpv), 293T cells were transfected with pCAGGP64, pCAGVSVG, and pFBASALF (provided by T. Miyazawa, Kyoto University), respectively; they were then infected with VSVΔG/Luc-*G, in which the G gene was replaced with the luciferase gene and was pseudotyped with the G protein (69), at a multiplicity of infection (MOI) of 0.1. The virus was adsorbed for 2 h at 37°C and extensively washed four times with serum-free DMEM. After 24 h of incubation at 37°C with DMEM-10% FBS, the culture supernatants were centrifuged to remove cell debris and stored at −80°C. The resulting VSV pseudotyped viruses transiently display heterologous or homologous envelope proteins. AcCAluc was generated by insertion of a luciferase gene under the control of the CAG promoter (40). Schematic representations of the recombinant baculovirus and the pseudotyped VSVs used in this study are shown below (see Fig. 2A). Recombinant baculovirus AcGP64TC, possessing a tetracysteine (TC) tag (Cys-Cys-Pro-Gly-Cys-Cys) at the N terminus of GP64, was generated by using a transfer vector, pAc-SURF2-TC, in which the TC tag sequence was cloned in frame under the signal sequence of GP64 of pBACsurf-1 (Merck KGaA, Darmstadt, Germany) by using the KpnI site (see Fig. 7A). AcGP64TC was then inoculated into Sf9 cells at an MOI of 0.1 and cultured in the presence of FlAsH-EDT2 (Invitrogen) (23). Culture supernatants were collected at 4 days postinfection, purified by sucrose gradient ultracentrifugation, and stored at −80°C.

Reagents. Chlorpromazine hydrochloride (CPZ), dynasore, lovastatin, MβCD, water-soluble cholesterol, and 5-*N*-ethyl-*N*-isopropyl amiloride (EIPA) were obtained from Sigma. Cells were preincubated with the drugs for 30 min (except for lovastatin) or 24 h (lovastatin) and infected with AcCAluc or pseudotyped VSV. In the MβCD treatment and cholesterol replenishment experiments, cells were cultured in DMEM with 10% lipid-free serum (BioWest, Nuaille, France). In the cholesterol replenishment experiments, cells were washed and incubated with DMEM containing water-soluble cholesterol for 30 min after treatment with Texas Red-labeled dextran, a marker of macropinocytosis (Invitrogen).

Determination of cellular cholesterol. MβCD-treated cells were washed with phosphate-buffered saline (PBS), and cellular cholesterol was determined as follows. Huh7 cells (10^6 cells/100 μl of PBS) were lysed by three cycles of freeze-thawing followed by sonication in a water bath sonicator (three bursts of 20 s each at 4°C). Cholesterol was extracted from the cell lysates by adding chloroform (200 μl) and methanol (100 μl) to the sonicated lysates (100 μl), and the bottom layer was collected and evaporated. The residual cholesterol was dissolved in ethanol and assayed using the Amplex Red cholesterol kit (Invitrogen).

Quantitative PCR. Entry and binding of baculovirus to cells were determined by quantitative PCR (qPCR). AcCAluc was incubated with cells for 30 min at 4°C or 37°C and then washed three times with PBS with or without 0.1% trypsin. The amount of baculovirus genome in the total cellular DNA (20 ng) was determined with Platinum SYBR green qPCR SuperMix (Invitrogen) using GP64-specific primers (5′-AGCTGATGTA

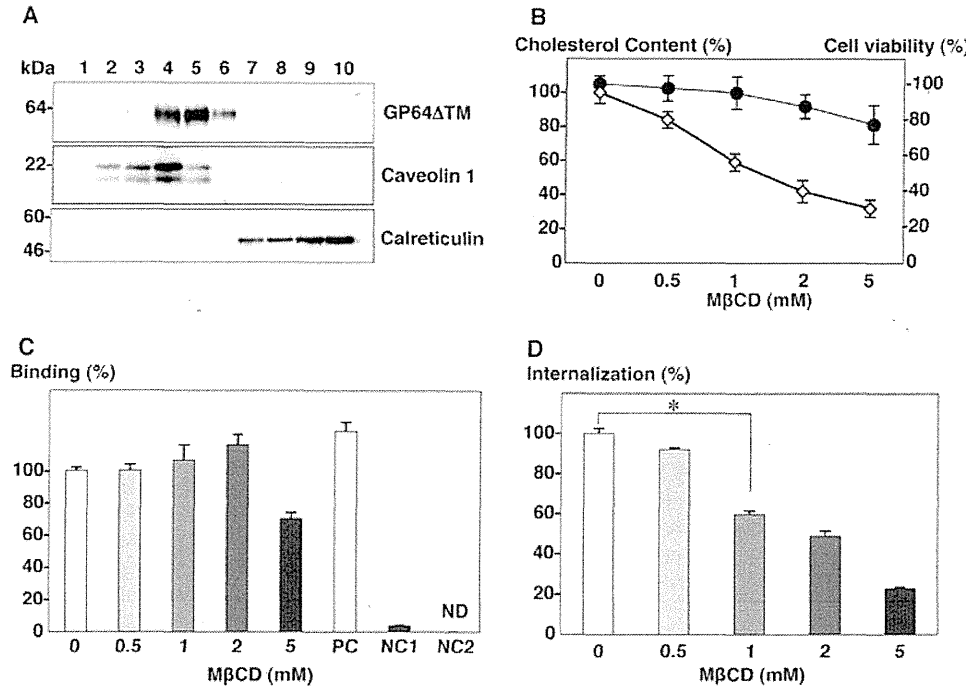

FIG 1 Cholesterol participates in the internalization of baculovirus into mammalian cells through direct interaction with GP64. (A) Huh7 cells were incubated with the purified GP64ΔTM at 4°C for 1 h, lysed with ice-cold lysis buffer, and subjected to a flotation assay. Aliquots of each fraction were assayed by Western blot analysis, which detected GP64ΔTM, caveolin-1, a lipid raft marker, and calreticulin, an endoplasmic reticulum marker. (B) The amount of cholesterol and the viability of Huh7 cells treated with various concentrations of MβCD for 30 min. The open diamonds and closed circles indicate the cholesterol content and cell viability, respectively. (C) Binding of AcCAluc to cholesterol-depleted Huh7 cells. Huh7 cells treated with various concentrations of MβCD were inoculated with AcCAluc at an MOI of 5, incubated at 4°C for 30 min, and washed three times with PBS, after which quantitative PCR determined the baculovirus genome in the total cellular DNA extracted from the cells (20 ng). PC represents viral genomes extracted from untreated Huh7 cells incubated with AcCAluc, NC1 represents viral genomes extracted from untreated cells washed three times with 0.1% trypsin-PBS after incubation with virus, and NC2 represents viral genomes extracted from mock-infected cells. ND, not detected. (D) Internalization of AcCAluc in MβCD-treated Huh7 cells. Huh7 cells treated with various concentrations of MβCD were inoculated with AcCAluc at an MOI of 5, incubated at 37°C for 30 min, and washed three times with 0.1% trypsin-PBS to remove the viral particles attached to the cell surface, after which quantitative PCR determined the intracellular viral genomes in the total cellular DNA extracted from the cells (20 ng). The results are the averages of three independent assays, with the error bars representing standard deviations (SD). *, $P < 0.05$.

CGAAAACGAT-3′ and 5′-TCGTGCAGCATATTGTTTAG-3′). Viral genomes extracted from Huh7 cells incubated with AcCAluc, those from cells washed three times with 0.1% trypsin-PBS after virus incubation, and those from mock-infected cells were used as a positive control (PC) and negative control 1 (NC1) and NC2, respectively.

Immunofluorescent staining. Cells cultured to be 50% confluent on a chambered slide were treated with chemicals or transfected with the plasmids and then inoculated with the viruses after incubation at 37°C for 24 h. The cells were fixed at 4°C for 30 min with 4% paraformaldehyde in PBS, permeabilized with 0.2% Triton X-100 in PBS for 5 min, and blocked with 1% bovine serum albumin (BSA) in PBS for 1 h at room temperature. The cells were reacted with appropriate primary antibodies diluted with 1% BSA in PBS for 1 h, followed by secondary antibodies; washed three times with PBS; and observed with a FluoView FV1000 laser scanning confocal microscope (Olympus, Tokyo, Japan).

Time-lapse microscopy. Huh7 cells were seeded at 1×10^3 cells in a μ-Dish (iBidi, Munich, Germany), grown overnight to 50% confluence, and incubated with FlAsH-labeled AcGP64TC at an MOI of 50 and with Texas Red-labeled dextran (2 mg/ml) at 4°C for 30 min. Internalization of the particles into living cells was observed at 37°C by laser scanning confocal microscopy. Digital images were analyzed with Image-Pro software (Media Cybernetics, Bethesda, MD).

Flotation assay. The flotation assay was described previously (30). Briefly, 2 million Huh7 cells were infected with AcCAluc or incubated with GP64ΔTM, lacking a transmembrane region, which was expressed in insect cells and purified as described previously (2) at 4°C. The cells were washed three times with ice-cold PBS, harvested with a rubber policeman, suspended in 500 μl of ice-cold TNE lysis buffer (25 mM Tris-HCl, pH 7.4, 150 mM NaCl, 5 mM EDTA, 0.1% Triton X-100), and incubated on ice for 30 min. The cell lysates were mixed with OptiPrep (Sigma) to 1 ml of a final concentration of 35%. This mixture was overlaid with 1 ml of 30%, 25%, and 10% OptiPrep, after which 0.5 ml of the lysis buffer was centrifuged at 40,000 rpm at 4°C for 16 h in an SW55Ti rotor (Beckman Coulter, Fullerton, CA). Each fraction was collected at 0.5 ml from the top of the centrifuge tube at 4°C. The fractions were subjected to immunoblotting.

Transfection and immunoblotting. The plasmids were transfected into cells using the FuGene 6 Transfection Reagent (Roche, Mannheim, Germany) according to the manufacturer's instructions. The protein samples were subjected to 12.5% sodium dodecyl sulfate-polyacrylamide gel electrophoresis (SDS-PAGE). The proteins were transferred to an Immobilon-P Transfer Membrane (Millipore, Tokyo, Japan) and were reacted with the appropriate antibodies. The immune complexes were visualized with Super Signal West Femto substrate (Pierce, Rockford, IL) and detected by an LAS-3000 image analyzer system (Fujifilm, Tokyo, Japan).

Statistical analysis. The results were expressed as means ± standard deviations. The significance of differences in the means was determined by Student's *t* test.

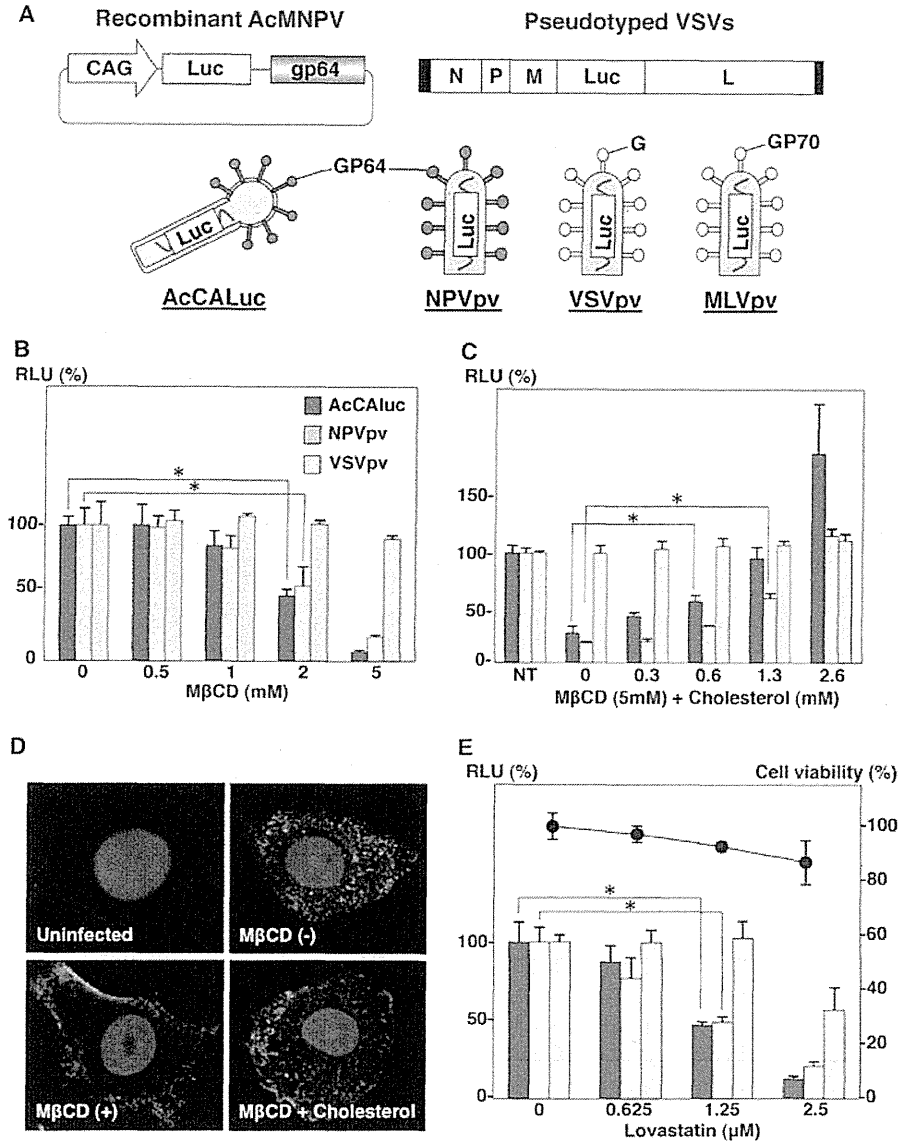

FIG 2 Cholesterol plays an important role in the internalization of baculovirus and the pseudotyped VSV bearing GP64. (A) Schematic representations of the recombinant baculovirus and the pseudotyped VSVs used in this study. Recombinant baculovirus AcCAluc has a luciferase gene under the control of the CAG promoter. The pseudotyped VSVs, NPVpv, VSVpv, and MLVpv, have a luciferase gene in place of the G gene and transiently display heterologous or homologous envelope proteins. (B) Huh7 cells were treated with various concentrations of MβCD for 30 min, followed by infection with AcCAluc (MOI, 5), NPVpv (MOI, 0.5), or VSVpv (MOI, 0.5), and the infectivity of each virus was determined in relative luciferase units (RLU) at 24 h postinfection. (C) Huh7 cells treated with 5 mM MβCD were replenished with various concentrations of water-soluble cholesterol for 30 min, followed by infection with the viruses; the infectivity of each virus was determined in RLU at 24 h postinfection. (D) Huh7 cells treated with 5 mM MβCD were incubated with AcCAluc at an MOI of 50 for 30 min. GP64 was stained with anti-GP64 antibody (AcV5) and Alexa Fluor 488-conjugated goat anti-mouse immunoglobulin G antibody after fixation with 4% paraformaldehyde, followed by permeabilization with 0.1% Triton X-100. Nuclei were stained with DAPI (4′,6-diamidino-2-phenylindole). (E) Huh7 cells were treated with various concentrations of lovastatin for 24 h, followed by inoculation with the viruses, and RLU and cell viability were determined at 24 h postinfection. The results are the averages of three independent assays, with the error bars representing SD. The bar and line graphs indicate RLU and cell viability, respectively. *, $P < 0.05$.

RESULTS

Cholesterol participates in the internalization of baculovirus into mammalian cells through direct interaction with GP64. A lipid raft is a microdomain on the cellular membrane and is sensitive to treatment with MβCD, which is a lipophilic cyclic oligosaccharide that is known to remove cholesterol from cellular membranes and to disrupt lipid raft formation (29). We have previously shown that GP64 expressed in mammalian cells was localized on the lipid rafts and that pseudotyped viruses bearing GP64 incorporated human decay-accelerating factor (DAF) during the budding process in mammalian cells (30). DAF is a membrane protein that regulates the complement system on the cell surface. To examine the direct interaction between GP64 and the lipid rafts during the entry process, a flotation assay was carried out by mixing purified GP64ΔTM protein, which lacks a transmembrane region, with Huh7 cells. The GP64ΔTM was detected

in fractions 3 to 6, which overlapped partially with those containing caveolin-1, a marker of lipid rafts (Fig. 1A), suggesting that the GP64ΔTM directly interacts with lipid rafts on the cell surface. We also performed this assay using AcCAluc, and GP64 was observed in the lipid raft fraction (data not shown). Next, to examine the role of cholesterol in the binding and internalization of baculovirus and pseudotyped viruses, Huh7 cells were treated with various concentrations of MβCD and then inoculated with AcCAluc bearing a luciferase gene under the CAG promoter. Treatment with MβCD, a chemical that depletes cholesterol (29), reduced the cellular cholesterol in Huh7 cells in a dose-dependent manner (Fig. 1B). Treatment with MβCD up to 2 mM exhibited no effect on virus binding, but 5 mM MβCD treatment showed 30% reduction. However, 5 mM MβCD treatment induced 20% reduction in living cells, as shown in Fig. 1B. In contrast, cholesterol reduction by MβCD treatment inhibited the internalization of AcCAluc into Huh7 cells in a dose-dependent manner (Fig. 1D). MβCD treatment clearly inhibited the internalization of AcCAluc in a dose-dependent manner, whereas 5 mM MβCD treatment exhibited a maximum 30% reduction in viral attachment and no dose dependency, suggesting that cholesterol participates mainly in the internalization of AcMNPV and slightly in its binding to mammalian cells.

Cholesterol plays important roles in the internalization of baculovirus and the pseudotyped VSV bearing GP64. To examine the role of cholesterol in GP64-mediated entry, Huh7 cells were treated with various concentrations of MβCD, and the viruses were then inoculated. MβCD treatment suppressed luciferase expression in cells inoculated with AcCAluc and NPVpv, but not with VSVpv, in a dose-dependent manner (Fig. 2B). Gene transduction in Huh7 cells upon infection with AcCAluc and NPVpv was reduced by approximately 50% and 90% by treatment with 2 mM and 5 mM MβCD, respectively. To confirm cholesterol's effect on the entry of the viruses, Huh7 cells treated with 5 mM MβCD were incubated with DMEM containing various concentrations of water-soluble cholesterol for 30 min and inoculated with the viruses. Internalization of viral DNA was recovered with AcCAluc, and NPVpv in the cholesterol-depleted cells was recovered by the replenishment of cholesterol in a dose-dependent manner (Fig. 2C). Next, we examined the effect of cholesterol on the entry of baculovirus by immunofluorescence microscopy (Fig. 2D). Although MβCD treatment dramatically reduced the detected level of GP64 in the cytoplasm, replenishment with cholesterol returned the level to comparability with that of the untreated cells. Finally, to confirm the effect of cholesterol on the internalization of baculovirus, Huh7 cells were treated with lovastatin, an inhibitor of cholesterol biosynthesis. Lovastatin treatment reduced the luciferase expression in cells inoculated with AcCAluc and NPVpv, but not in those inoculated with VSVpv, in a dose-dependent manner (Fig. 2E). Collectively, these results suggest that cholesterol plays an important role in the internalization of AcMNPV and the pseudotyped viruses bearing GP64 into mammalian cells.

Baculovirus and pseudotyped VSV bearing GP64 internalize into mammalian cells through an endosome. There are conflicting reports on the entry of AcMNPV suggesting that baculovirus internalizes into cells through a clathrin-dependent endocytic pathway (40, 44) or a clathrin-independent and phagocytosis-like endocytic pathway (36). To determine whether AcMNPV and the pseudotyped viruses internalize into cells through endosomes,

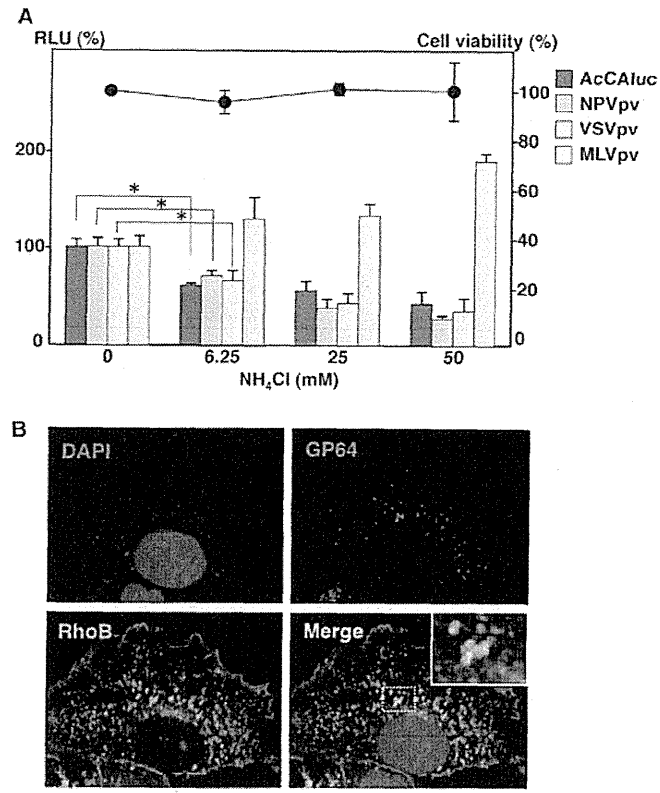

FIG 3 Baculovirus is internalized into mammalian cells through an endosome. (A) Huh7 cells were treated with various concentrations of NH_4Cl for 30 min, followed by infection with AcCAluc (MOI, 5), NPVpv (MOI, 0.5), VSVpv (MOI, 0.5), or MLVpv (MOI, 0.5), and RLU and cell viability were determined at 24 h postinfection. The results are the averages of three independent assays, with the error bars representing SD. The bar and line graphs indicate RLU and cell viability, respectively. *, $P < 0.05$. (B) Huh7 cells expressing GFP-fused RhoB were infected with AcCAluc at an MOI of 50 for 45 min. GP64 was stained with anti-GP64 antibody (AcV5) and Alexa Fluor 594-conjugated goat anti-mouse immunoglobulin G antibody after fixation with 4% paraformaldehyde, followed by permeabilization with 0.1% Triton X-100. Nuclei were stained with DAPI. The boxed region in the merged image is magnified in the inset.

Huh7 cells were treated with ammonium chloride (NH_4Cl), an inhibitor of endosome acidification. Luciferase expression in cells inoculated with AcCAluc, NPVpv, and VSVpv was reduced by treatment with NH_4Cl in a dose-dependent manner, in contrast to cells infected with MLVpv, which enters cells through a direct fusion between viral and plasma membranes at neutral pH (Fig. 3A). Next, to determine the subcellular localization of baculovirus, infected Huh7 cells expressing GFP-fused RhoB, an endosome marker, were stained with anti-GP64 antibody (AcV5). The colocalization of GP64 and RhoB was detected by confocal microscopy (Fig. 3B). These results support the notion that AcMNPV and the pseudotyped VSV bearing GP64 internalize into mammalian cells through endocytosis.

Dynamin participates in the internalization of baculovirus and the pseudotyped VSV bearing GP64. We further examined the roles of the molecules essential for endocytosis, including dynamin, clathrin, and caveolin, in the GP64-mediated internalization of viral particles. The role of dynamin, a large GTPase promoting fission of the endocytic membrane and a pivotal factor in

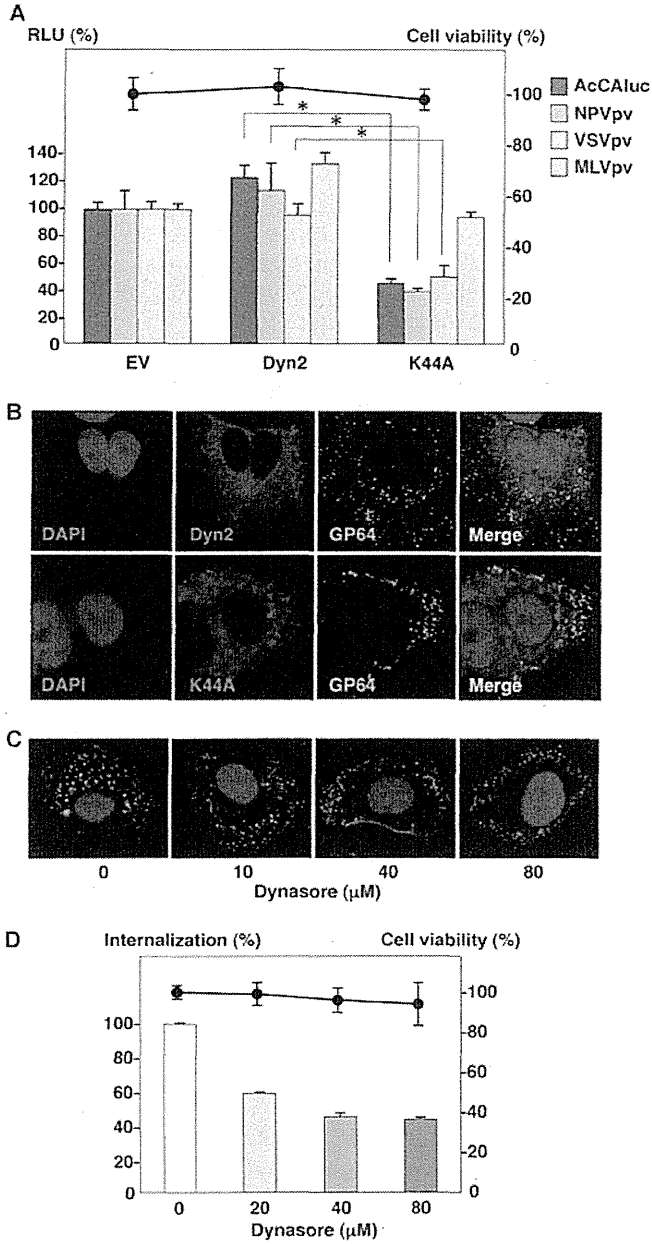

FIG 4 Dynamin participates in the internalization of baculovirus and the pseudotyped VSV bearing GP64. (A) Huh7 cells transfected with EV or plasmids encoding the wild type or a dominant-negative mutant (K44A) of Dyn2 were infected with AcCAluc (MOI, 5), NPVpv (MOI, 0.5), VSVpv (MOI, 0.5), or MLVpv (MOI, 0.5). The RLU and cell viability were determined at 24 h postinfection. The results are the averages of three independent assays, with the error bars representing SD. The bar and line graphs indicate RLU and cell viability, respectively. *, $P < 0.05$. (B) Huh7 cells were transfected with plasmids encoding either HA-Dyn2 or HA-K44A and were infected with AcCAluc at an MOI of 50 at 24 h posttransfection. HA-Dyn2 and HA-K44A were stained with rabbit antibodies against HA- and Alexa Fluor 594-conjugated goat anti-rabbit immunoglobulin G antibody. GP64 was stained with anti-GP64 antibody (AcV5) and Alexa Fluor 488-conjugated goat anti-mouse immunoglobulin G antibody. Nuclei were stained with DAPI. (C) Huh7 cells were treated with various concentrations of dynasore for 30 min, followed by infection with AcCAluc at an MOI of 50. GP64 was stained with anti-GP64 antibody (AcV5) and Alexa Fluor 488-conjugated goat anti-mouse immunoglobulin G antibody after fixation with 4% paraformaldehyde, followed by permeabilization with 0.1% Triton X-100. Nuclei were stained with DAPI. (D) Huh7 cells treated with various concentrations of dynasore for 30 min were incubated with AcCAluc at an MOI of 50 at 37°C for 30 min, after which cell viability was determined. The cells were washed three times with 0.1% trypsin-PBS to remove the viral particles attached to the cell surface, and intracellular viral genomes in the total cellular DNA extracted from the cells (20 ng) were determined by quantitative PCR. The results are the averages of three independent assays, with the error bars representing SD. The bar and line graphs indicate RLU and cell viability, respectively. *, $P < 0.05$.

endocytosis, was determined by using a dominant-negative mutant of dynamin (K44A) and dynasore, an inhibitor of dynamin. Expression of an HA-tagged dynamin mutant (K44A) inhibited the gene transduction of AcCAluc, NPVpv, and VSVpv, but not that of MLVpv, compared to the empty vector (EV) or the wild-type (WT) HA-tagged dynamin (Dyn2) (Fig. 4A). Huh7 cells that expressed either HA-tagged wild-type or K44A mutant dynamin or that had been treated with various concentrations of dynasore were inoculated with AcCAluc and examined by immunofluorescence microscopy after immunostaining. Expression of the K44A mutant, but not of wild-type dynamin, inhibited the internalization of baculovirus (Fig. 4B), and treatment with dynasore also reduced the internalization of the viruses in a dose-dependent manner (Fig. 4C and D), indicating that dynamin participates in the internalization of baculovirus and the pseudotyped VSV bearing GP64.

Clathrin-dependent and caveola-independent endocytoses participate in GP64-mediated viral entry into mammalian cells. Both clathrin- and caveola-dependent endocytoses utilize dynamin. Therefore, we next examined the involvement of these pathways in GP64-mediated entry. The dominant-negative mutant of caveolin-1, $CAV1^{DGV}$, was shown to inhibit caveola-mediated endocytosis (61). Expression of $CAV1^{DGV}$ (Fig. 5A) and the knockdown of caveolin-1 by small interfering RNA (siRNA) targeted to caveolin-1 (Fig. 5B) exhibited no significant effect on gene transduction in Huh7 cells upon infection with AcCAluc and the pseudotyped VSVs, suggesting that caveola-mediated endocytosis is not required for GP64-mediated viral entry. Next, we examined the involvement of clathrin in GP64-mediated entry. Treatment with CPZ, an inhibitor of clathrin-mediated endocytosis, inhibited the gene transduction of AcCAluc, NPVpv, and VSVpv, but not that of MLVpv, in a dose-dependent manner (Fig. 5C). In immunofluorescence analysis, CPZ treatment abrogated the internalization of GP64 into Huh7 cells (Fig. 5D). Eps15, which localizes in the clathrin-coated pit, is a key factor in clathrin-mediated endocytosis (5, 72). Expression of a dominant-negative mutant of Eps15 (Δ95-295) produced a 40% reduction in gene transduction of AcCAluc, NPVpv, and VSVpv but no reduction in that of MLVpv (Fig. 5E). These results suggested that baculovirus and the pseudotyped VSV bearing GP64 internalize into mammalian cells through clathrin-dependent and caveola-independent endocytoses.

Macropinocytosis participates in GP64-mediated viral entry into mammalian cells. Baculovirus is 40 to 50 nm in diameter and 200 to 400 nm in length (64), while the clathrin-coated pit is about 100 to 150 nm in diameter. Therefore, baculovirus particles are likely a little too large for uptake by clathrin-mediated endocytosis. To determine the role of macropinocytosis in the entry of baculovirus, Huh7 cells were treated with various concentrations of EIPA, an inhibitor of Na^+/H^+ ion exchange and filopodium formation, after which they were inoculated with the viruses. Treatment with EIPA inhibited the gene transduction of AcCAluc

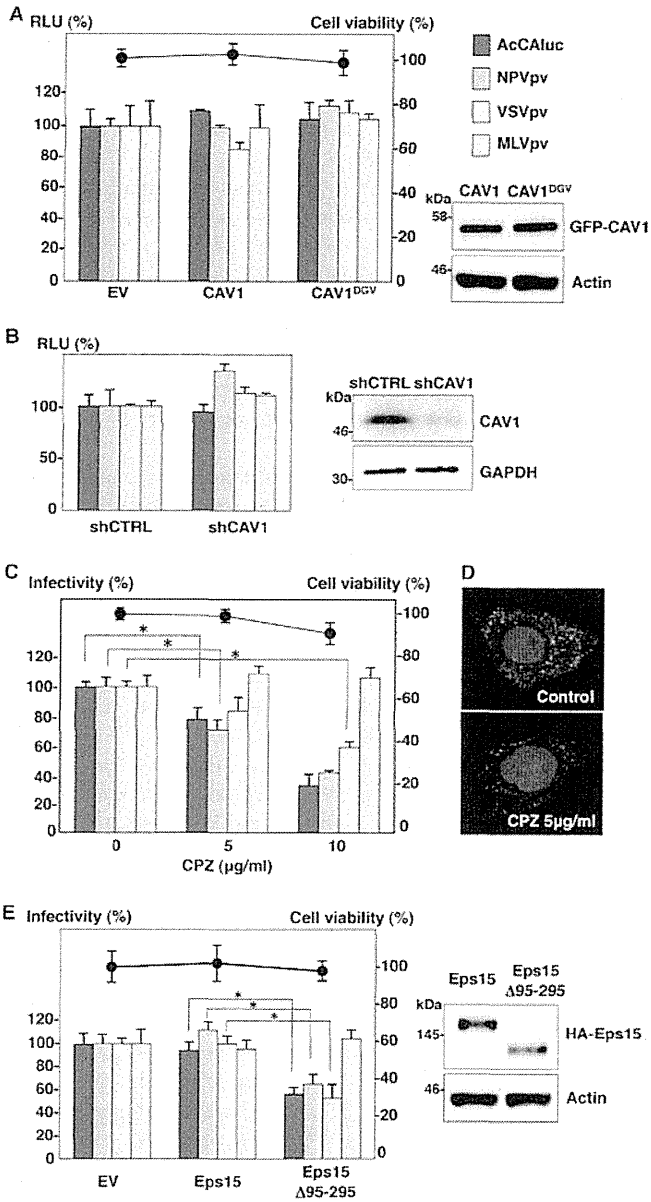

FIG 5 Clathrin-dependent and caveola-independent endocytosis is involved in GP64-mediated viral entry into mammalian cells. (A) (Left) Huh7 cells transfected with plasmids encoding either GFP, GFP-fused CAV1, or GFP-fused CAV1^{DGV} were infected with AcCAluc (MOI, 5), NPVpv (MOI, 0.5), VSVpv (MOI, 0.5), or MLVpv (MOI, 0.5), and RLU and cell viability were determined at 24 h postinfection. (Right) Expression of the GFP fusion CAV1 proteins was determined by immunoblotting. (B) (Left) The knockdown cells were infected with AcCAluc (MOI, 5), NPVpv (MOI, 0.5), VSVpv (MOI, 0.5), or MLVpv (MOI, 0.5). The RLU were determined at 24 h postinfection. (Right) Huh7 cells transfected with plasmids encoding shRNA targeted to CAV1 (shCAV1) or nonspecific targets (shCTRL) were cultivated for 2 days in the presence of hygromycin and lysed with buffer containing 1% Triton X-100. Expression of CAV1 and actin was detected by immunoblotting. (C) Huh7 cells were treated with various concentrations of CPZ for 30 min, followed by infection with AcCAluc (MOI, 5), NPVpv (MOI, 0.5), VSVpv (MOI, 0.5), or MLVpv (MOI, 0.5), and the RLU and cell viability were determined at 24 h postinfection. (D) Huh7 cells treated with 5 μg/ml of CPZ were incubated with AcCAluc at an MOI of 50 for 30 min. GP64 was stained with anti-GP64 antibody (AcV5) and Alexa Fluor 488-conjugated goat anti-mouse immunoglobulin G antibody after fixation with 4% paraformaldehyde, followed by permeabilization with 0.1% Triton X-100. Nuclei were stained with DAPI. (E) Huh7 cells transfected with EV or plasmids encoding the wild type or a dominant-negative mutant (Δ95-295) of Eps15 were infected with AcCAluc (MOI, 5), NPVpv (MOI, 0.5), VSVpv (MOI, 0.5), or MLVpv (MOI, 0.5). The RLU and cell viability were determined at 24 h postinfection. The results are the averages of three independent assays, with the error bars representing SD. The bar and line graphs indicate RLU and cell viability, respectively. *, $P < 0.05$.

most efficiently, followed by that of NPVpv, in a dose-dependent manner, whereas it had no effect on that of VSVpv and MLVpv (Fig. 6A). Rab34 has been shown to be involved in the formation of macropinosomes (67), and the expression of a dominant-negative mutant of Rab34 (T66N) in Huh7 cells inhibited gene transduction of AcCAluc and NPVpv, but not that of VSVpv or MLVpv (Fig. 6B). In the immunofluorescence assay, treatment with EIPA reduced the internalization of both baculovirus and dextran in a dose-dependent manner (Fig. 6C and data not shown). These results indicate that macropinocytosis also participates in the internalization of baculovirus and that GP64 *per se* is capable of inducing macropinocytosis.

Live imaging of the internalization of baculovirus into mammalian cells. To examine the internalization of baculovirus by live-cell imaging, we generated a recombinant baculovirus possessing tetracysteine-tagged GP64 (AcGP64TC) (Fig. 7A). The labeled tetracysteine tag allows imaging of the location of the protein. The labeled AcGP64TC and Texas Red-labeled dextran were incubated with Huh7 cells. The labeled GP64 was incorporated into cells together with dextran (Fig. 7B) over time. These results support the notion that macropinocytosis also participates in the internalization of baculovirus into mammalian cells.

DISCUSSION

Baculovirus has a large capacity to incorporate foreign genes and exhibits a broad spectrum for internalization into mammalian cells but low cytotoxicity due to a lack of replication; thus, baculovirus is thought to be a promising viral-vector candidate for future human gene therapy (16, 34, 73). Baculovirus GP64 has been shown to participate in attachment to both insect and mammalian cells, as well as in the low-pH-triggered membrane fusion following endocytosis (7, 8, 14, 16, 19, 28, 36, 38, 49, 50, 75). Although the mechanisms of entry of AcMNPV have not been well characterized, previous studies suggested that AcNMPV enters cells through a clathrin-dependent (40, 44) or -independent (36) endocytic pathway. In this study, we utilized a recombinant baculovirus possessing a luciferase gene under the control of a mammalian promoter and pseudotyped viruses bearing envelope glycoproteins of AcMNPV, VSV, and MLV to facilitate more reliable and quantitative analyses of GP64-mediated entry into mammalian cells. The resultant data suggest that cholesterol participates in the internalization of baculovirus but not in its binding to mammalian cells and that baculovirus is internalized into cells through clathrin-dependent but caveola-independent endocytosis or macropinocytosis.

We reported previously that the entry of AcMNPV into mammalian cells was inhibited by treatment with either phosphatidylethanolamine or phosphatidylinositol and was reduced in mutant hamster cell lines deficient in phospholipid biosynthesis (70). We also previously showed that incorporation of human DAF into viral particles through interaction with GP64 in the lipid raft confers resistance to the viral particles bearing GP64 against serum

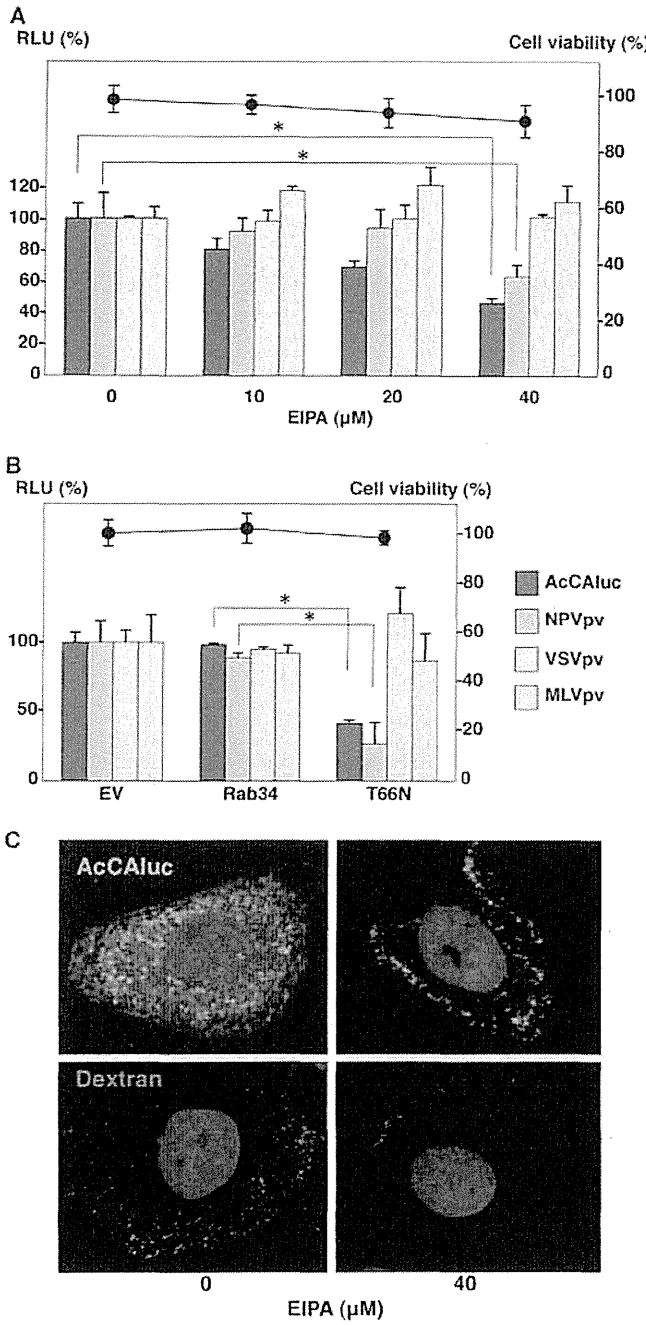

FIG 6 Macropinocytosis participates in GP64-mediated viral entry into mammalian cells. (A) Huh7 cells were treated with various concentrations of EIPA for 30 min, followed by infection with AcCAluc (MOI, 5), NPVpv (MOI, 0.5), VSVpv (MOI, 0.5), or MLVpv (MOI, 0.5), and RLU and cell viability were determined at 24 h postinfection. The results are the averages of three independent assays, with the error bars representing SD. *, $P < 0.05$. (B) Huh7 cells transfected with EV or plasmids encoding the wild type or a dominant-negative mutant (T66N) of Rab34 were infected with AcCAluc (MOI, 5), NPVpv (MOI, 0.5), VSVpv (MOI, 0.5), or MLVpv (MOI, 0.5). The RLU and cell viability were determined at 24 h postinfection. The bar and line graphs indicate RLU and cell viability, respectively. *, $P < 0.05$. (C) Huh7 cells were treated with 40 μm of EIPA for 30 min, followed by incubation with either AcCAluc at an MOI of 50 or Texas Red-labeled dextran (2 mg/ml). GP64 was stained with anti-GP64 antibody (AcV5) and Alexa Fluor 488-conjugated goat anti-mouse IgG antibody after fixation with 4% paraformaldehyde, followed by permeabilization with 0.1% Triton X-100. Nuclei were stained with DAPI.

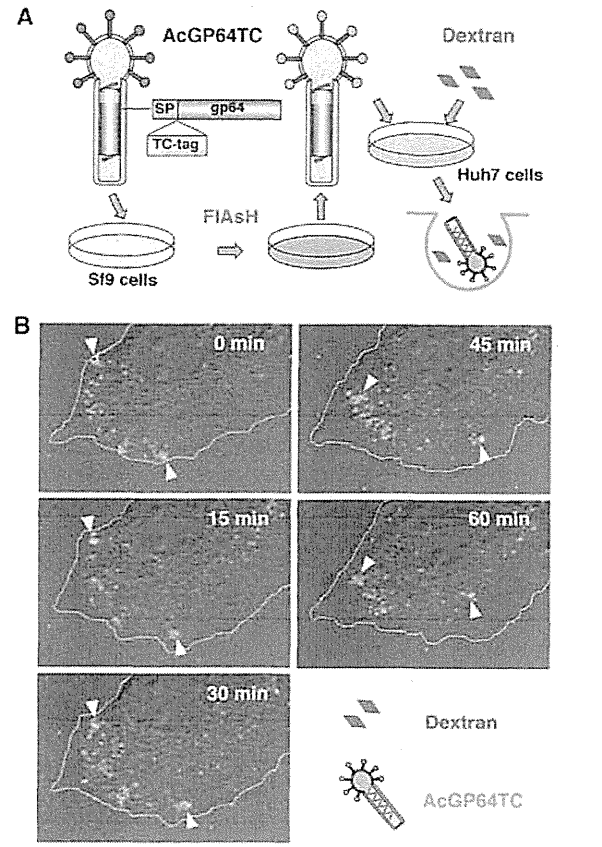

FIG 7 Live images of internalization of the recombinant baculovirus into mammalian cells. (A) AcGP64TC incorporates the TC tag sequence (Cys-Cys-Pro-Gly-Cys-Cys) under the signal peptide sequence (SP) in the N terminus of the mature GP64. The flanking amino acid sequences are -Ala-Asp-Leu-Gln- and -Pro-Arg-Ala-Glu-. Sf9 cells were infected with AcGP64TC at an MOI of 0.1 and cultured in the presence of FlAsH-EDT2 for 4 days, and the labeled viral particles were incubated with Huh7 cells at 4°C for 30 min, together with Texas Red-labeled dextran as a marker of macropinocytosis. The temperature was then raised to 37°C for examination of the internalization of the particles in the living cells by confocal microscopy. (B) Time-lapse images of the internalization of FlAsH-labeled AcGP64TC (green), together with dextran (red), into Huh7 cells. Internalization of the particles into cells was viewed at 37°C by confocal microscopy.

inactivation (30). The lipid raft plays crucial roles in signal transduction, protein sorting, and membrane transport (9, 66). Clustering of the lipid rafts was shown to be essential for the signaling cascade (51, 66). In this study, we have shown that the depletion and inhibition of the biosynthesis of cholesterol by treatment with MβCD and lovastatin, respectively, impaired GP64-dependent internalization but not the binding of the viruses. Phosphatidylserine (PS), which is localized in the inner plasma membrane, is known to be exposed on the envelopes of viral particles of vaccinia virus and HIV (10, 46). Morizono et al. reported that the serum-soluble protein Gas6 binds to both PS on viral particles and TAM receptor tyrosine kinase Axl on target cells and mediates virus binding by bridging the virus to target cells (52). Because Gas6-dependent entry is not limited by a specific interaction between viral envelope proteins and cell surface receptors, this alternative pathway may broaden the host range and enhance the infectivity of various envelope viruses. Infection with pseudotyped Sindbis

virus bearing baculovirus GP64 to human microvascular endothelial cells was shown to be enhanced by treatment with Gas6 (51). However, our treatment with Gas6 had no effect on gene transduction by baculovirus and NPVpv into both Huh7 and A549 cells expressing low and high levels of Axl, respectively (data not shown). Differences of pseudotyped virus, VSV based or Sindbis based, might raise this discrepancy. Further studies are needed to clarify the involvement of cholesterol in the lipid raft in the internalization of baculovirus into mammalian cells.

Many enveloped viruses have been shown to internalize into cells through an endocytosis pathway. Clathrin-mediated endocytosis is involved in the internalization of viruses and receptors through a clathrin-coated pit (100 to 150 nm in diameter). The pit buds into the cytosol and delivers a virus first to the early endosomes and then to the late endosomes and lysosomes (25). Many molecules participate in this process, such as Dyn2, Eps15, and accessory protein 2 (13). A number of viruses, including VSV, influenza virus, and hepatitis C virus, are known to use this pathway for entry (6, 54, 68, 76). Conflicting data have been published concerning the involvement of clathrin-dependent endocytosis in the internalization of baculovirus into mammalian cells (36, 40, 44, 63). To obtain more reliable data, in this study, we examined GP64's role in the entry into mammalian cells by using the pseudotyped VSV bearing GP64, together with the pseudotypes possessing envelope glycoproteins of VSV and MLV, as viral controls for entry through the endocytic pathway and direct fusion, respectively. VSV is known to internalize into target cells through clathrin-mediated endocytosis, and the G glycoprotein of VSV exhibits characteristics similar to those of baculovirus GP64 (22). The data obtained in this study support the notion that AcMNPV is internalized into mammalian cells through clathrin-dependent endocytosis (36, 40, 44, 63).

Caveolin-mediated endocytosis, a different form of clathrin-mediated endocytosis, is known to be used by simian virus 40 (57). Caveolae are the caveolin-coated and flask-shaped membrane invaginations associated with lipid rafts (35, 37). Caveolin-1 is typically found in the lipid raft fraction of plasma membranes and is essential for caveola formation through interaction with cholesterol. For a molecule to be internalized through caveolin-mediated endocytosis, it must be no larger than 50 to 80 nm, the diameter of a flask-shaped caveola. Both clathrin- and caveolin-mediated endocytoses require dynamin, a large GTPase promoting the fission of the endocytic membrane (27). The expression of a dominant-negative mutant of caveolin-1 and the suppression of caveolin-1 did not affect the internalization of baculovirus; this is consistent with previous reports suggesting that baculovirus is internalized into mammalian cells through the lipid raft microdomain in the caveola-independent pathway (36, 40, 44).

Macropinocytosis is associated with membrane raffles driven by actin polymerization, such as filopodia and lamelipodia, and has been studied mainly in antigen presentation and the uptake of extracellular fluid and solids, as well as particles, such as bacteria, apoptotic cell fragments, and viruses (21, 31). Viruses, such as Ebola virus, vaccinia virus, coxsackievirus, herpes simplex virus (HSV), and HIV, are reported to use macropinocytosis to enter target cells (18, 42, 47, 48, 53, 62). Macropinocytosis is a transient, growth-factor-induced, actin-dependent endocytic process that leads to the internalization of fluid and membrane in large vacuoles. Like the factors involved in other endocytic mechanisms, structural changes in the plasma membrane during macropinocytosis are tightly regulated by many factors, including the Na^+/H^+ exchanger, Rho GTPase family, and protein kinase C (PKC) (48). In this study, macropinocytosis appeared to participate in the internalization of baculovirus into mammalian cells, based on data obtained by treatment with EIPA, an inhibitor of the Na^+/H^+ exchanger; by the expression of the dominant-negative mutant of Rab34, which is involved in macropinosome closure; and by the time-lapse microscopic observation of the tetracystein-tagged AcMNPV, in contrast to the previous observation (36). This discrepancy might be attributable to the differences in cell types and assay systems. Furthermore, the expression of a dominant-negative mutant of Rab34 suppressed gene transduction in cells infected, not only with AcCAluc, but also with NPVpv (Fig. 6B), suggesting that the interaction of GP64 with the cellular receptor(s) triggers macropinocytosis, as seen in infection with Ebola virus (53, 62).

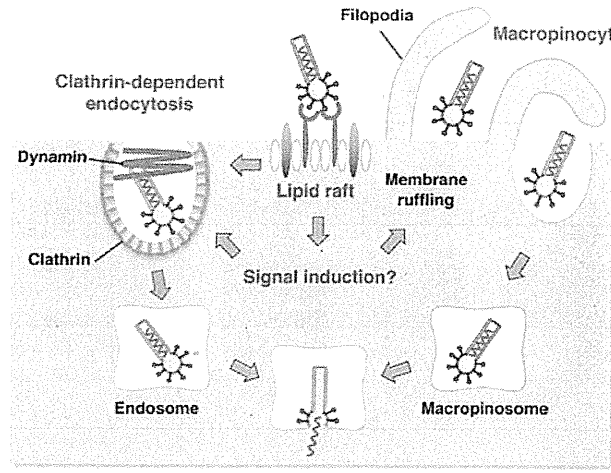

FIG 8 Putative model of internalization of baculovirus into mammalian cells. Baculovirus binds to a not-yet-identified cellular receptor(s) present in the lipid raft. This association induces cellular remodeling through signal transduction. In clathrin-mediated endocytosis, baculovirus is internalized into the clathrin-coated pit. In macropinocytosis, filopodia formed by actin dynamics wrapped the baculovirus into a macropinosome. The viral genome is released from the endosome or macropinosome through membrane fusion induced by low pH.

The data in this study suggest that baculovirus interacts with the molecules on the lipid raft via GP64 and then is internalized through clathrin-mediated endocytosis and macropinocytosis. This pathway is reminiscent of the entry of EGF receptor, which localizes in the caveola-containing lipid rafts (59), exits from the lipid rafts upon interaction with EGF, and is internalized into cells through clathrin-mediated endocytosis (39). A hypothetical model of baculovirus entry into mammalian cells based on data in the present and previous studies is shown in Fig. 8. In this model, baculovirus binds to a not-yet-identified cellular receptor(s) present in the lipid rafts, this association induces cellular remodeling through signal transduction, and baculovirus is internalized into cells through clathrin-mediated endocytosis and macropinocytosis.

Baculovirus is known to use heparan sulfate on the cell surface as an attachment factor (20). In a recent study, Wu and Wang identified the sequence in GP64 responsible for binding to heparin, and this binding is essential for baculovirus internalization into mammalian cells (78). Although there are many studies on

baculovirus entry, no baculovirus entry receptors have been identified yet. Since baculovirus is capable of internalizing into various cells originating from not only insects, but also mammals, baculovirus would utilize ubiquitously distributed or multiple molecules to enter the cells. The data presented in this study should provide clues for the future development of baculovirus vectors suitable for efficient and specific gene delivery into target cells and tissues.

ACKNOWLEDGMENTS

We thank H. Murase and M. Tomiyama for their secretarial work. We also thank T. Miyazawa for providing plasmids.

This work was supported in part by grants-in-aid from the Ministry of Health, Labor, and Welfare; the Ministry of Education, Culture, Sports, Science, and Technology; and the Osaka University Global Center of Excellence Program.

The funders had no role in study design, data collection and analysis, decision to publish, or preparation of the manuscript.

REFERENCES

1. Abe T, et al. 2005. Involvement of the Toll-like receptor 9 signaling pathway in the induction of innate immunity by baculovirus. J. Virol. 79:2847–2858.
2. Abe T, et al. 2009. Baculovirus induces type I interferon production through Toll-like receptor-dependent and -independent pathways in a cell-type-specific manner. J. Virol. 83:7629–7640.
3. Abe T, et al. 2003. Baculovirus induces an innate immune response and confers protection from lethal influenza virus infection in mice. J. Immunol. 171:1133–1139.
4. Bavari S, et al. 2002. Lipid raft microdomains: a gateway for compartmentalized trafficking of Ebola and Marburg viruses. J. Exp. Med. 195: 593–602.
5. Benmerah A, Bayrou M, Cerf-Bensussan N, Dautry-Varsat A. 1999. Inhibition of clathrin-coated pit assembly by an Eps15 mutant. J. Cell Sci. 112:1303–1311.
6. Blanchard E, et al. 2006. Hepatitis C virus entry depends on clathrin-mediated endocytosis. J. Virol. 80:6964–6972.
7. Blissard GW, Wenz JR. 1992. Baculovirus gp64 envelope glycoprotein is sufficient to mediate pH-dependent membrane fusion. J. Virol. 66:6829–6835.
8. Boyce FM, Bucher NL. 1996. Baculovirus-mediated gene transfer into mammalian cells. Proc. Natl. Acad. Sci. U. S. A. 93:2348–2352.
9. Brown DA, London E. 2000. Structure and function of sphingolipid- and cholesterol-rich membrane rafts. J. Biol. Chem. 275:17221–17224.
10. Callahan MK, et al. 2003. Phosphatidylserine on HIV envelope is a cofactor for infection of monocytic cells. J. Immunol. 170:4840–4845.
11. Carbonell LF, Klowden MJ, Miller LK. 1985. Baculovirus-mediated expression of bacterial genes in dipteran and mammalian cells. J. Virol. 56:153–160.
12. Chen BJ, Leser GP, Morita E, Lamb RA. 2007. Influenza virus hemagglutinin and neuraminidase, but not the matrix protein, are required for assembly and budding of plasmid-derived virus-like particles. J. Virol. 81:7111–7123.
13. Chen H, et al. 1998. Epsin is an EH-domain-binding protein implicated in clathrin-mediated endocytosis. Nature 394:793–797.
14. Chernomordik L, Leikina E, Cho MS, Zimmerberg J. 1995. Control of baculovirus gp64-induced syncytium formation by membrane lipid composition. J. Virol. 69:3049–3058.
15. Chung CS, Huang CY, Chang W. 2005. Vaccinia virus penetration requires cholesterol and results in specific viral envelope proteins associated with lipid rafts. J. Virol. 79:1623–1634.
16. Condreay JP, Kost TA. 2007. Baculovirus expression vectors for insect and mammalian cells. Curr. Drug Targets 8:1126–1131.
17. Condreay JP, Witherspoon SM, Clay WC, Kost TA. 1999. Transient and stable gene expression in mammalian cells transduced with a recombinant baculovirus vector. Proc. Natl. Acad. Sci. U. S. A. 96:127–132.
18. Coyne CB, Shen L, Turner JR, Bergelson JM. 2007. Coxsackievirus entry across epithelial tight junctions requires occludin and the small GTPases Rab34 and Rab5. Cell Host Microbe 2:181–192.
19. Dong S, et al. 2010. Autographa californica multicapsid nucleopolyhedrovirus efficiently infects Sf9 cells and transduces mammalian cells via direct fusion with the plasma membrane at low pH. J. Virol. 84:5351–5359.
20. Duisit G, et al. 1999. Baculovirus vector requires electrostatic interactions including heparan sulfate for efficient gene transfer in mammalian cells. J. Gene Med. 1:93–102.
21. Falcone S, et al. 2006. Macropinocytosis: regulated coordination of endocytic and exocytic membrane traffic events. J. Cell Sci. 119:4758–4769.
22. Garry CE, Garry RF. 2008. Proteomics computational analyses suggest that baculovirus GP64 superfamily proteins are class III penetrenes. Virol. J. 5:28.
23. Griffin BA, Adams SR, Tsien RY. 1998. Specific covalent labeling of recombinant protein molecules inside live cells. Science 281:269–272.
24. Gronowski AM, Hilbert DM, Sheehan KC, Garotta G, Schreiber RD. 1999. Baculovirus stimulates antiviral effects in mammalian cells. J. Virol. 73:9944–9951.
25. Gruenberg J. 2001. The endocytic pathway: a mosaic of domains. Nat. Rev. Mol. Cell Biol. 2:721–730.
26. Hefferon KL, Oomens AG, Monsma SA, Finnerty CM, Blissard GW. 1999. Host cell receptor binding by baculovirus GP64 and kinetics of virion entry. Virology 258:455–468.
27. Henley JR, Krueger EW, Oswald BJ, McNiven MA. 1998. Dynamin-mediated internalization of caveolae. J. Cell Biol. 141:85–99.
28. Hofmann C, et al. 1995. Efficient gene transfer into human hepatocytes by baculovirus vectors. Proc. Natl. Acad. Sci. U. S. A. 92:10099–10103.
29. Ilangumaran S, Hoessli DC. 1998. Effects of cholesterol depletion by cyclodextrin on the sphingolipid microdomains of the plasma membrane. Biochem. J. 335:433–440.
30. Kaname Y, et al. 2010. Acquisition of complement resistance through incorporation of CD55/decay-accelerating factor into viral particles bearing baculovirus GP64. J. Virol. 84:3210–3219.
31. Kerr MC, Teasdale RD. 2009. Defining macropinocytosis. Traffic 10: 364–371.
32. Kitagawa Y, et al. 2005. Ligand-directed gene targeting to mammalian cells by pseudotype baculoviruses. J. Virol. 79:3639–3652.
33. Kitajima M, et al. 2008. Induction of natural killer cell-dependent antitumor immunity by the Autographa californica multiple nuclear polyhedrosis virus. Mol. Ther. 16:261–268.
34. Kost TA, Condreay JP. 2002. Recombinant baculoviruses as mammalian cell gene-delivery vectors. Trends Biotechnol. 20:173–180.
35. Kurzchalia TV, Parton RG. 1999. Membrane microdomains and caveolae. Curr. Opin. Cell Biol. 11:424–431.
36. Laakkonen JP, et al. 2009. Clathrin-independent entry of baculovirus triggers uptake of E. coli in non-phagocytic human cells. PLoS One 4:e5093.
37. Lajoie P, Nabi IR. 2010. Lipid rafts, caveolae, and their endocytosis. Int. Rev. Cell Mol. Biol. 282:135–163.
38. Leikina E, Onaran HO, Zimmerberg J. 1992. Acidic pH induces fusion of cells infected with baculovirus to form syncytia. FEBS Lett. 304:221–224.
39. Le Roy C, Wrana JL. 2005. Clathrin- and non-clathrin-mediated endocytic regulation of cell signalling. Nat. Rev. Mol. Cell Biol. 6:112–126.
40. Long G, Pan X, Kormelink R, Vlak JM. 2006. Functional entry of baculovirus into insect and mammalian cells is dependent on clathrin-mediated endocytosis. J. Virol. 80:8830–8833.
41. Luckow VA, Summers MD. 1988. Signals important for high-level expression of foreign genes in Autographa californica nuclear polyhedrosis virus expression vectors. Virology 167:56–71.
42. Maréchal V, et al. 2001. Human immunodeficiency virus type 1 entry into macrophages mediated by macropinocytosis. J. Virol. 75:11166–11177.
43. Markovic I, Pulyaeva H, Sokoloff A, Chernomordik LV. 1998. Membrane fusion mediated by baculovirus gp64 involves assembly of stable gp64 trimers into multiprotein aggregates. J. Cell Biol. 143:1155–1166.
44. Matilainen H, et al. 2005. Baculovirus entry into human hepatoma cells. J. Virol. 79:15452–15459.
45. Matsuura Y, Possee RD, Overton HA, Bishop DH. 1987. Baculovirus expression vectors: the requirements for high level expression of proteins, including glycoproteins. J. Gen. Virol. 68:1233–1250.
46. Mercer J, Helenius A. 2010. Apoptotic mimicry: phosphatidylserine-mediated macropinocytosis of vaccinia virus. Ann. N. Y. Acad. Sci. 1209: 49–55.
47. Mercer J, Helenius A. 2008. Vaccinia virus uses macropinocytosis and apoptotic mimicry to enter host cells. Science 320:531–535.